United States
Environmental Protection
Agency

Office of Research and
Development
Washington DC 20460

EPA/600/R-99/104
September 1999

Hydrogeologic Foundations in Support of Ecosystem Restoration: Base-flow Loadings of Nitrate in Mid-Atlantic Agricultural Watersheds

EPA/600/R-99/104
September 1999

Hydrogeologic Foundations in Support of Ecosystem Restoration: Base-flow Loadings of Nitrate in Mid-Atlantic Agricultural Watersheds

Mohamed M. Hantush
Subsurface Protection and Remediation Division
National Risk Management Research Laboratory
Ada, OK 74820

Jerome Cruz
ManTech Environmental Research Services Corp.
Ada, OK 74820

National Risk Management Research Laboratory
Office of Research and Development
U.S. Environmental Protection Agency
Cincinnati, OH 45268

Notice

The U.S. Environmental Protection Agency through its Office of Research and Development funded the research described here through inhouse efforts. The data used in this analysis was provided by the U.S. Geological Survey under IAG #DW14937941. This report has been subjected to the Agency's peer and administrative review and has been approved for publication as an EPA document. Mention of trade names or commercial products does not constitute endorsement or recommendation for use.

All research projects making conclusions or recommendations based on environmentally related measurements and funded by the Environmental Protection Agency are required to participate in the Agency Quality Assurance Program. This project was conducted under an approved Quality Assurance Project Plan. The procedures specified in this plan were used without exception. Information on the plan and documentation of the quality assurance activities and results are available from the Principal Investigator.

Foreword

The U.S. Environmental Protection Agency is charged by Congress with protecting the Nation's land, air, and water resources. Under a mandate of national environmental laws, the Agency strives to formulate and implement actions leading to a compatible balance between human activities and the ability of natural systems to support and nurture life. To meet these mandates, EPA's research program is providing data and technical support for solving environmental problems today and building a science knowledge base necessary to manage our ecological resources wisely, understand how pollutants affect our health, and prevent or reduce environmental risks in the future.

The National Risk Management Research Laboratory is the Agency's center for investigation of technological and management approaches for reducing risks from threats to human health and the environment. The focus of the Laboratory's research program is on methods for the prevention and control of pollution to air, land, water, and subsurface resources; protection of water quality in public water systems; remediation of contaminated sites and ground water; and prevention and control of indoor air pollution. The goal of this research effort is to catalyze development and implementation of innovative, cost-effective environmental technologies; develop scientific and engineering information needed by EPA to support regulatory and policy decisions; and provide technical support and information transfer to ensure effective implementation of environmental regulations and strategies.

This publication has been produced as part of the Laboratory's strategic long-term ecosystem restoration research plan, and in fulfillment of the Division (SPRD) FY99 GPRA Goals and Measures.

Clinton W. Hall, Director
Subsurface Protection and Remediation Division
National Risk Management Research Laboratory

Abstract

Field evidence suggests that deep denitrification in the subsurface has the potential for removal of nitrate from ground water. Two adjacent agricultural watersheds in the mid-Atlantic coastal plain display remarkable differences in their ground-water nitrate discharges. It is believed that a combination of denitrification in reducing subsurface sediments and historical nitrogen input variations are responsible for the observed behavior. The process of deep denitrification may be influenced by geohydrologic factors, including the regional dip of strata in the mid-Atlantic coastal plain. A multi-scale-modeling framework is being developed for analysis and assessment of nitrate removal by denitrification in reducing subsurface sediments in riparian zones. Analytical characteristic solutions are derived for general transects in watersheds, and regional ground-water and nitrate transport and fate models are being developed. Preliminary assessment based on the characteristic solutions predicts a potential for more than 60 percent reduction of ground-water nitrate at the discharge to Morgan Creek and 20 percent reduction at the Chesterville Branch. This may be attributed to a shallower zone of reducing sediments (redox zone) below the former, where a significant fraction of ground-water fluxes that enter this zone are assumed to be denitrified, and a relatively deeper redox zone below the latter, whereby a greater portion of ground-water flux may escape denitrification before discharging to surface water. The analysis may have overpredicted ground-water nitrate loadings to the Chesterville Branch, possibly due to overlooking potential denitrification in the peat-rich riparian stream-valley sediments. Although predictions are consistent with field findings, more intensive sampling would be required to resolve deep denitrification from potential removal within riparian stream-valley sediments. Simple indices are derived on the basis of steady-state mass balance, which describe the removal capacity for ground-water nitrate in agricultural watersheds. The indices relate the reduction in nitrate base-flow loading to potential denitrification in the subsurface in agricultural catenments and stream riparian zones. A regional ground-water surface water flow model has been developed in order to investigate the impact of denitrification in ground water at the watershed scale. The simulated ground-water levels and stream discharges compared very well with quasi-steady synoptic measurements of heads in the surficial Columbia-Aquia aquifer and the lower Hornerstown aquifer. The measured stream flows in Morgan Creek are reproduced by the simulated values. The regional flow model is a prelude to analysis of regional nitrate transport and fate and assessment of the potential impact of deep denitrification on nitrate budget in the paired watersheds, including total mass discharge to the Chester River. This report covers a period from 10/01/97 to 08/01/99 and work was completed as of 08/01/99.

Contents

Figures

Tables

Acknowledgments

This project was initiated by Dr. S. R. Kraemer, U.S. Environmental Protection Agency, including the development of original work and quality assurance plans. Dr. D. Krantz, Dr. J. L. Bachman, and Dr. J. K. Böhlke of the U.S. Geological Survey developed and executed the field work plan and assisted in the interpretation of new hydrostratigraphic and geochemical data. Dr. D. Drummond of the Maryland Geological Survey provided existing hydrostratigraphic data for the construction of the geologic model. Mr. E. Hoque of ManTech Environmental Research Services Corp. assisted in the regional ground-water flow modeling effort. Ms. K. Tynsky and Ms. M. Williams of Orbiting Astronomical Observatory Corp. provided graphical support and developed the final format of the report. We thank Dr. M. Mariño, Dr. R. Govindaraju, Dr. K. Bali, and Dr. J. Cho for their reviews and valuable comments.

1. Introduction

Chesapeake Bay, the United States' largest and most productive estuary, faces several complex environmental issues, including, among others, eutrophication and anoxia in the main channel and tributaries (*Cronin et al,. 1999*). The outbreak of the toxic dinoflagellate *Pfiesteria piscicida* is linked to nutrient enrichment in the Chesapeake Bay. Agriculture was identified as a major contributor of nutrients to the Chesapeake Bay in the 1987 Chesapeake Bay Agreement. Under this agreement, the states of Maryland, Pennsylvania, and Virginia, and the District of Columbia committed to a 40 percent nutrient load reduction to the Chesapeake Bay by the year 2000 (*U.S. Environmental Protection Agency*, 1992). It is imperative to estimate base flow loading since much of the nitrogen that is discharged to the bay and its tidal tributaries is transported by ground water as base flow or direct discharge (*Bachman and Phillips*, 1996). Improper management of nutrients can result in losses to ground water by leaching and surface water by runoff. Therefore, nutrient management through rate, timing, and mode of application can prevent pollution and reduce their potential losses through runoff or leaching to ground water.

Riparian buffer zones and constructed wetlands are potential natural filters and are proposed as a nutrient management method. In the design of riparian buffer areas, the subsurface environment, including the stream valley sediments, and the interaction between surface and ground water are as important as the size of buffer zone and species composition. The role of the subsurface as an integral compartment of the riparian zone needs to be emphasized and evaluated for possible impact as a nutrient management method. Figure 1 shows paired predominantly agricultural watersheds in the mid-Atlantic coastal plain. The area is located in Kent County, Maryland, and the two watersheds, the Morgan Creek and the Chesterville Branch, although adjacent, show remarkably different nitrate levels in their base flows. Based on geochemical analysis, it was reported by *Böhlke and Denver* (1995) that the concentrations of nitrate (NO_3^-) in ground-

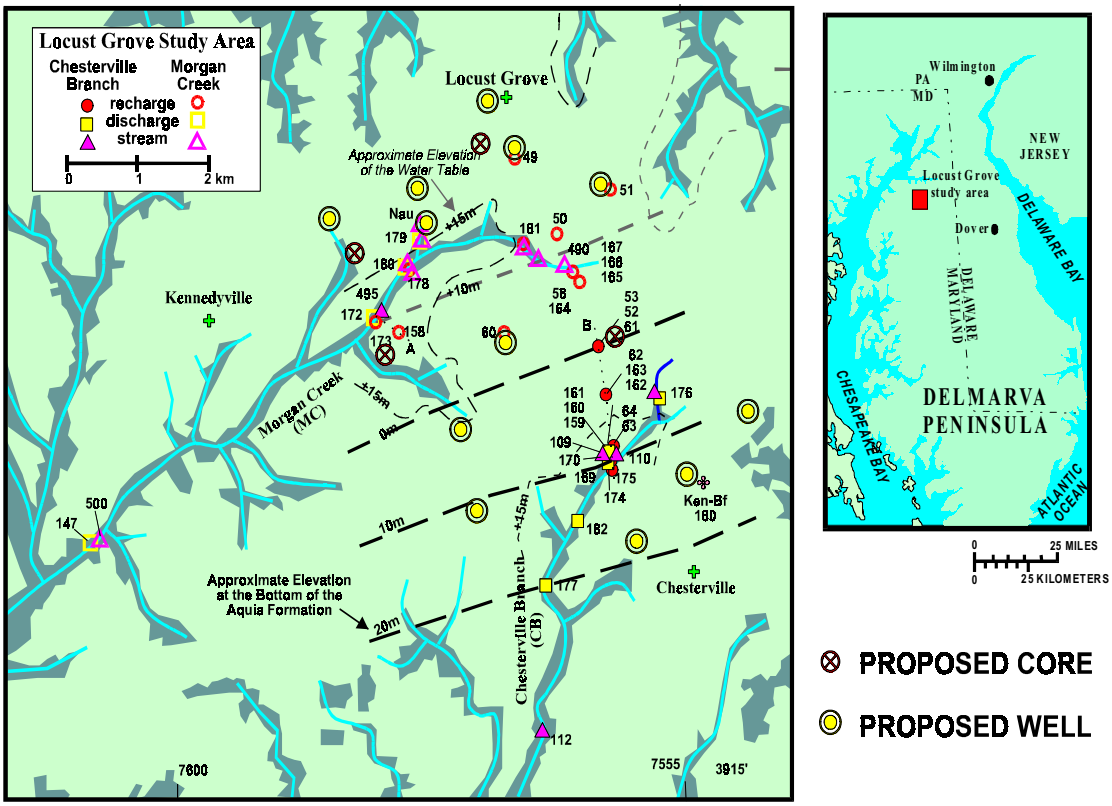

Figure 1. Locust Grove study site with location of proposed core holes and wells (after Böhlke and Denver, 1995).

water discharge to the Morgan Creek were significantly lower than in the Chesterville Branch (Figure 2). It is believed that a combination of deep denitrification (microbial reduction of NO_3^- to N_2) in reducing subsurface sediments and historical input variations is responsible for the observed behavior. The difference in the position of the redox zone (brown-shaded in Figure 2) relative to the bottom of each streambed produced by the regional dip of the strata, combined with the ground-water flow pattern, may be responsible for greater denitrification in ground waters discharging to the Morgan Creek.

Nitrogen removal in riparian zones has been investigated in shallow ground waters (*Yates and Sheridan*, 1983; *Lowrance et al.*, 1984; *PeterJohn and Correll*, 1984; *Jacobs and Gilliam*, 1985; and *Cooper*, 1990). Recently, the impact of redox reactions (e.g., microbial denitrification) on nitrate removal in deeper ground waters has been the subject of several studies (*Trudell et al.*, 1986; *Postma et al.*, 1991; *Kinzelbach et al.*, 1991; *Korom*, 1992; *Böhlke and Denver*, 1995; and *Mengis et al.*, 1999), which indicated the role of denitrification in ground water on the reduction of nitrate discharge to riparian streams. While most efforts are field based and focused on mass balance of nitrogen over an entire area of study, mechanistic models that describe transient transport and fate of nitrate in ground water (e.g., *Kinzelbach et al.*, 1991) received less attention. This may be attributed to the complexity of nitrogen transformation and uncertainty associated with the subsurface environment, which is further compounded by lack of a detailed geohydrologic and geochemical data base.

The current study is a consortium between the U.S. Environmental Protection Agency (National Risk Management Research Laboratory) and the U.S. Geological Survey (Baltimore and Dover). The objectives of this study are: 1) to develop a geohydrological database for paired agricultural watersheds shown in Figure 1; and, 2) to develop a scale-dependent methodology for the assessment of the effectiveness of deep denitrification on the reduction of nitrate discharge to riparian streams. The goal is to provide an adaptable framework with implication on the design of the riparian zones and management of nitrogen in agricultural watersheds.

In the following sections the geohydrological foundation is developed for the assessment of nitrate transport and fate at the local as well as the regional scale. At the local scale, a framework is developed which describes ground-water flow in inclined, unconfined aquifers with implication on nitrate fate and transport in agroecosystem. The purpose of the local-scale models is to provide a foundation, using basic physics, for understanding the impact of deep denitrification on ground-water discharge, and to provide a viable reasoning for the observed disparity of base-flow nitrate levels at the two watersheds. At the regional scale, the ground-water flow model is developed for the watersheds and application results are displayed. The regional transport model, however, is not addressed in this report and is currently under development.

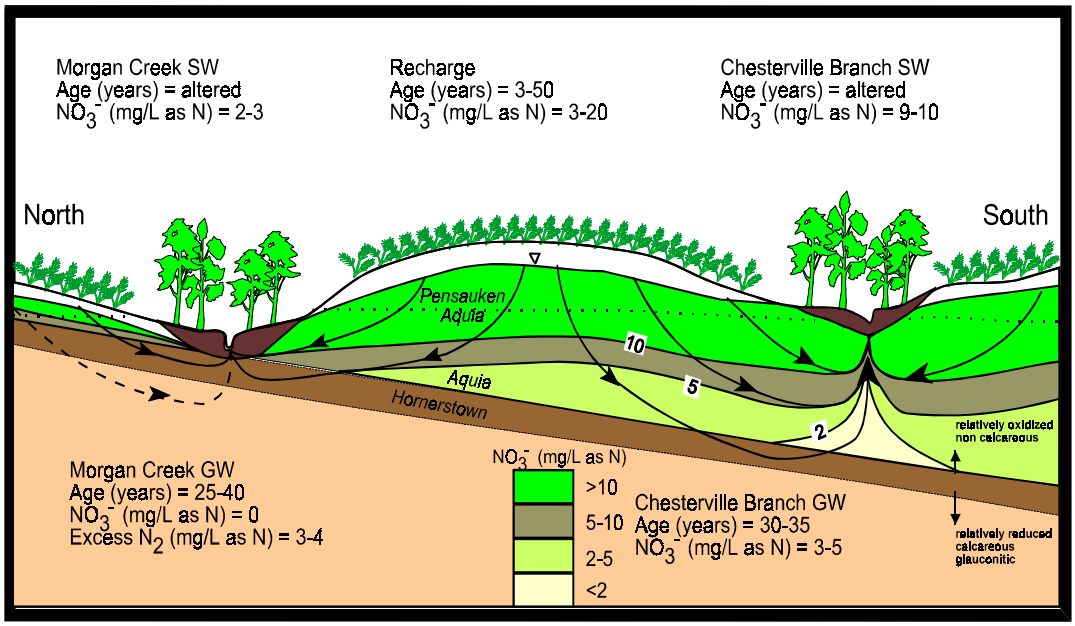

Figure 2. Generalized geologic cross section through Locust Grove, Maryland (after Böhlke and Denver, 1995).

2. Theoretical Foundation

2.1 Ground-water Flow in Unconfined Aquifer

In the following sections we develop analytical solutions which describe one-dimensional and steady-state water table elevations and ground-water fluxes in an inclined, unconfined (phreatic) aquifer subject to uniform recharge. The solutions should enable the estimation of ground-water fluxes from the upper oxic layer to the lower anoxic layer and ground-water discharge (base flow) to a stream. The lower anoxic layer denotes the zone of reducing sediments in the catchment under study, in which nitrate is believed to be partially or entirely denitrified before discharging to Morgan Creek and the Chesterville Branch. An approximate solution to the nonlinear exact solution will be obtained using asymptotic expansions and will be used in determining transport and fate of nitrate nitrogen in the subsurface. Among other factors, the impact of aquifer bed inclination is also considered in the solutions.

2.1.1 Water Table Distribution

Figure 3 illustrates a conceptual stream-aquifer system for Morgan Creek in which the aquifer bed is inclined with a positive angle measured relative to a horizontal plane at a reference elevation (or datum) of the aquifer bed at the right-hand-side boundary. Ground-water flow toward the stream occurs due to a uniform recharge of magnitude N [m/d] and a prescribed influx Q_0 [m^3/d] at the right-hand-side boundary at x = 0 m (Figure 3). A water divide at x = 0, corresponds to the special case of $Q_0 = 0$. The steady-state flow in the unconfined aquifer may be described by the following *Dupuit* equation (*Bear*, 1972):

$$\frac{d}{dx}\left(K\eta(x)\frac{dh}{dx}\right) + N = 0 \tag{1}$$

where

$$h(x) = \eta(x) + \beta\, x \tag{2}$$

in which h(x) is the hydraulic head at steady state [m]; η(x) is steady-state water table elevation relative to the aquifer bed [m]; K is the hydraulic conductivity [m/d] assumed to be constant; β = tan θ is the gradient of aquifer bed; N is the uniform recharge [m/d]; and *x* is the horizontal distance. Equation (1) is valid for sufficiently small β so that *Dupuit's*

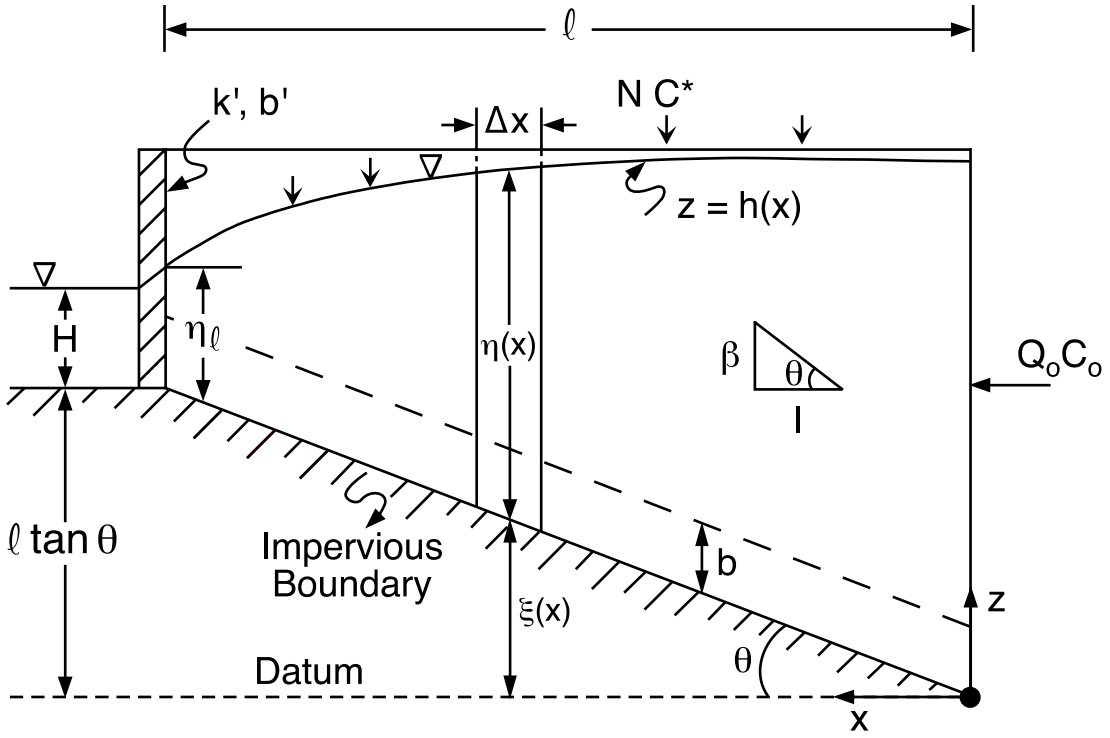

Figure 3. Conceptual model for the Morgan Creek: Unconfined aquifer with positive inclination.

assumption of horizontal flow in the aquifer is applicable. We seek a solution to (1) subject to the following boundary conditions:

$$-K\eta\frac{dh}{dx}=Q_0, \qquad x=0 \tag{3a}$$

$$-K\eta\frac{dh}{dx}=K'[W/2+h-H_r]\frac{\eta-H}{b'}, \qquad x=l \tag{3b}$$

in which K' is the hydraulic conductivity of the streambed [m/d]; b' is the thickness of the streambed deposits [m] (i.e., semipervious boundary layer); W is the stream width [m]; H_r is the streambed elevation relative to datum (m); and H is the stream stage relative to aquifer bed at $x = l$. Streambed conductance $K'/b' = \infty$ corresponds to the special case of perfect hydraulic connection between the stream and the aquifer. Note that in (3b), $W/2+h(l)-H_r$ is the ground-water surface water discharge area per unit aquifer width, at $x = l$. It is based on the assumption that ground water is intercepted entirely by the stream and that no horizontal flow occurs below the stream.

Using the linear transformation $\xi = N x + Q_0$, the solution to the above boundary-value problem (1-3) is shown in detail in Appendix A:

$$\frac{\eta^2+(\beta/N)\eta(Nx+Q_0)+(1/KN)(Nx+Q_0)^2}{\eta_l^{\,2}+(\beta/N)\eta_l(Nl+Q_0)+(1/KN)(Nl+Q_0)^2}=\exp\left\{-\frac{\beta}{\gamma N}\left[\tan^{-1}\left(\frac{\eta_l/(Nl+Q_0)+\beta/(2N)}{\gamma}\right)-\tan^{-1}\left(\frac{\eta(x)/(Nx+Q_0)+\beta/(2N)}{\gamma}\right)\right]\right\} \tag{4}$$

where

$$\gamma=\sqrt{\frac{1}{KN}-\frac{\beta^2}{4N^2}} \tag{5}$$

The integration of Equation (1) and the imposition of boundary condition (3b) yield

$$\eta_l=H-\frac{1}{2}\left(\frac{W}{2}+H-H_r+\beta l\right)+\frac{1}{2}\sqrt{\left(\frac{W}{2}+H-H_r+\beta l\right)^2+4\frac{Nl+Q_0}{K'/b'}} \tag{6}$$

in which η_l is water table elevation above the streambed at $x = l$ [m]. Equation (4) requires that $\gamma \geq 0$, whereas for negative net recharge (i.e., evapotranspiration greater than infiltration), we have $\gamma < 0$ and $-\tan^{-1}(\bullet)$ in Equation (4) should be replaced by $+\coth^{-1}(\bullet)$.

Note that (4) is nonlinear with respect to the dependent variable η and can be solved using a standard iterative procedure for solving nonlinear equations, such as the Newton Raphson method. A useful approximate but closed-form solution to (4) can be obtained for sufficiently small $\beta << 1$ using a straightforward expansion in the form of a power series in β (e.g., *Nayfeh*, 1981):

$$\eta(x)=\phi_0(x)+\beta\phi_1(x)+\beta^2\phi_2(x)+\ldots\ldots, \qquad \beta<<1 \tag{7}$$

in which $\phi_0(x)$, $\phi_1(x)$, ..etc, are to be identified. In the expansion (7) the function $\phi_0(x)$ corresponds to the case of a horizontal bed, and $\phi_1(x)$ represents a correction due to a small inclination of the aquifer bed. It is usually sufficient to retain the first two terms (zero- and first-order) and ignore higher order terms of $O[\beta^2]$ and greater. By substituting the right-hand-side of (7) into (4) and collecting terms of equal order in β, one can show that:

$$\phi_0(x) = \sqrt{\eta_l^{\,2} + \frac{1}{K\,N}\left[(N\,l + Q_0)^2 - (N\,x + Q_0)^2\right]} \tag{8}$$

and

$$\phi_1(x) = \frac{1}{2\,\phi_0(x)}\left\{\frac{\eta_l}{N}(N\,l + Q_0) - \left(\eta_l^{\,2} + \frac{(N\,l + Q_0)^2}{K\,N}\right)\left[\tan^{-1}\left(\sqrt{KN}\,\frac{\eta_l}{N\,l + Q_0}\right) - \tan^{-1}\left(\sqrt{KN}\,\frac{\phi_0(x)}{N\,x + Q_0}\right)\right]\right\} - \frac{1}{2\,N}(N\,x + Q_0) \tag{9}$$

Not only do Equations (7-9) provide an approximate closed-form solution to the nonlinear head distribution in (4), but also, as will be evident later in the analysis, they enable an analytical closed-form solution for nitrate transport in ground water and allow for direct assessment of the impact of the denitrification in the reducing subsurface sediments on nitrogen reduction in riparian buffer zones; i.e., potential reduction of nitrate in the discharge (base flows) to the Morgan Creek and the Chesterville Branch.

2.1.2 Ground-water Flux in Oxic and Redox Zones

In this analysis the upper layer is referred to as oxic in order to indicate that ground waters remain oxic throughout the upper layer and, therefore, discharge relatively unaltered to streams (*Böhlke and Denver*, 1995), and the lower layer is referred to as redox to represent the reduction-oxidation process of denitrification in the reducing sediments of the lower layer. The total ground-water flux $Q_T(x)$ over a flow depth of (x) is given by the integration of Dupuit's Equation (1) from x = 0 to x = x**,** which yields

$$Q_T(x) = N\,x + Q_0 \tag{10}$$

In Dupuit's equation, equipotential lines are assumed to be vertical and ground-water flow is essentially horizontal. Thus, the flux in the lower (redox) layer of thickness b (Figure 3) is given by

$$Q_l(x) = \frac{b}{\eta(x)}\,Q_T(x) \tag{11}$$

The flux in the upper oxic layer is given by

$$Q_u(x) = \frac{\eta(x) - b}{\eta(x)}\,Q_T(x) \tag{12}$$

Note that $dQ_l(x)/dx$ represents ground-water flux from the upper layer to the lower one by virtue of continuity of flow in and out of an incremental control volume of V = b x. That is, any increase in the flow rate in the lower layer (redox zone) must be balanced out by transfer of ground-water flow from the upper (oxic) layer. This is an important part of the problem under consideration, because $dQ_l(x)/dx$ describes the rate at which nitrate is convected to the redox zone and, consequently, lost out of the system by denitrification in the reducing sediments before discharging to the riparian streams.

A direct use of (11) and (12) is not possible because of the nonlinearity of (4) with respect to η(x), and an iterative procedure, therefore, is needed for the flux evaluation. However, a closed-form approximate solution can be obtained by substituting the asymptotic expansion on the right-hand-side of (7) for η(x) in Equations (11) and (12) and collecting and equating terms of equal order of magnitude with respect to the parameter β,

$$Q_l(x) \approx \frac{b}{\phi_0(x)}\left(N\,x + Q_0\right)\left(1 - \frac{\phi_1(x)}{\phi_0(x)}\beta\right) \tag{13}$$

and

$$Q_u(x) \approx \left(N\,x + Q_0\right)\left(1 - \frac{b}{\phi_0(x)} + b\frac{\phi_1(x)}{\left[\phi_0(x)\right]^2}\beta\right) \tag{14}$$

Figure 4 is a mirror image to the flow scenario in the Chesterville Branch depicted in Figure 2 where the gradient of the aquifer bed is negative and ground-water flow pathways are longer. In this case, ground-water flux is progressively distributed over greater flow areas and a significant fraction of the ground water escapes the lower (redox) layer before discharging to the stream. The solutions in the previous case of positive aquifer bed gradient are equally applicable to the case of negative gradient, however, with the parameter β being negative. This is because the methodology above is applicable for a general inclination angle θ, and for the Chesterville Branch, the only difference is that θ is negative relative to the horizontal line which passes through the origin at the base of the aquifer at the water divide. In the case of Morgan Creek, θ is positive relative to the horizontal reference level.

2.2 Nitrate Transport and Fate in Ground Water

In the following sections, the governing transport and fate equations for nitrate are developed for each layer using the concept of conservation of mass. The resulting equation for the upper (oxic) layer is then solved analytically using a characteristic solution in terms of the functions $\phi_0(x)$ and $\phi_1(x)$. If the nitrate-nitrogen is assumed to be denitrified instantly in the lower (redox) layer (*Böhlke and Denver*, 1995), then base-flow loading from the upper layer is the only source of nitrate discharged to both streams. In this case, the solution of the transport equation in the upper layer is sufficient to describe nitrate reduction at the discharging waters, because all nitrate convected to the lower layer would presumably be lost out of the riparian system by denitrification in the reducing sediments. If denitrification occurs at a finite rate, rather than instantly, the solution for the transport equation in the redox layer becomes necessary since nitrate is partially denitrified, and the discharge from the lower layer to the streams would contribute nitrate discharge

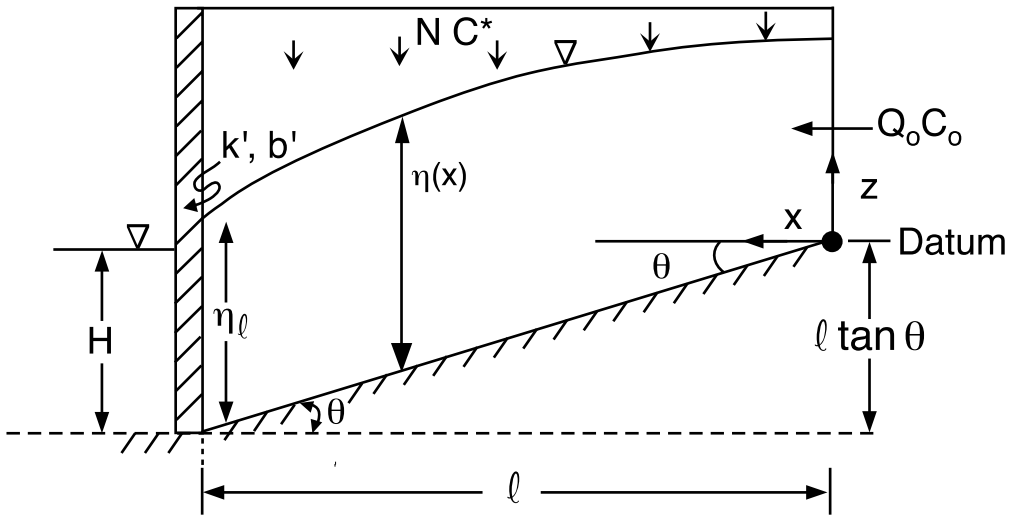

Figure 4. Conceptual model for the Chesterville Branch: Unconfined aquifer with negative inclination.

to the stream. The solution for nitrate transport and fate in the lower layer under the condition of partial denitrification is currently under investigation.

2.2.1 Development of Transport Equations

2.2.1.1 Upper Layer (Oxic Zone)

Figure 5 shows a control volume tapping the aquifer at distance x of length Δx and height η(x) per unit width of the aquifer. The upper layer is of thickness η - b and the lower layer is of thickness b. Mass balance of a contaminant through the upper layer in the control volume requires that

$$\text{Mass at time } t+\Delta t = \text{Mass at time } t + \text{Mass In during } \Delta t$$
$$- \text{Mass Out during } \Delta t - \text{Rate of Loss} \times \Delta t \qquad (15)$$

If we ignore production of nitrate within the control volume and assume convective transport (i.e., negligible dispersive effects), then for infinitesimal Δx and Δt, the application of (15) to mass balance in the upper-layer portion of the control volume (Figure 5) yields

$$n(\eta - b)\Delta x\, C_u(x, t+\Delta t) - n(\eta - b)\Delta x C_u(x,t) = N\, C^*(x,t)\Delta x \Delta t + Q_u(x) C_u(x,t)\Delta t$$
$$- n(\eta - b)\Delta x\, k_u\, C_u(x,t)\Delta t - \frac{dQ_l}{dx}\Delta x C_u(x,t)\Delta t - Q_u(x+\Delta x) C_u(x+\Delta x, t)\Delta t \qquad (16)$$

in which C_u is the concentration of nitrate in the upper layer [g/m^3]; n is aquifer porosity; $C^*(x,t)$ is concentration of nitrate at the recharge [g/ m^3]; and k_u is a first-order rate loss coefficient [d^{-1}], which accounts for partial denitrification. In Equation (16), we assumed uniform concentration throughout the depth η-b and, therefore, convective losses of magnitude C_u to the lower-layer portion at a rate of dQ_l/dx x (the fourth term on the right-hand side of (16)). Recall that

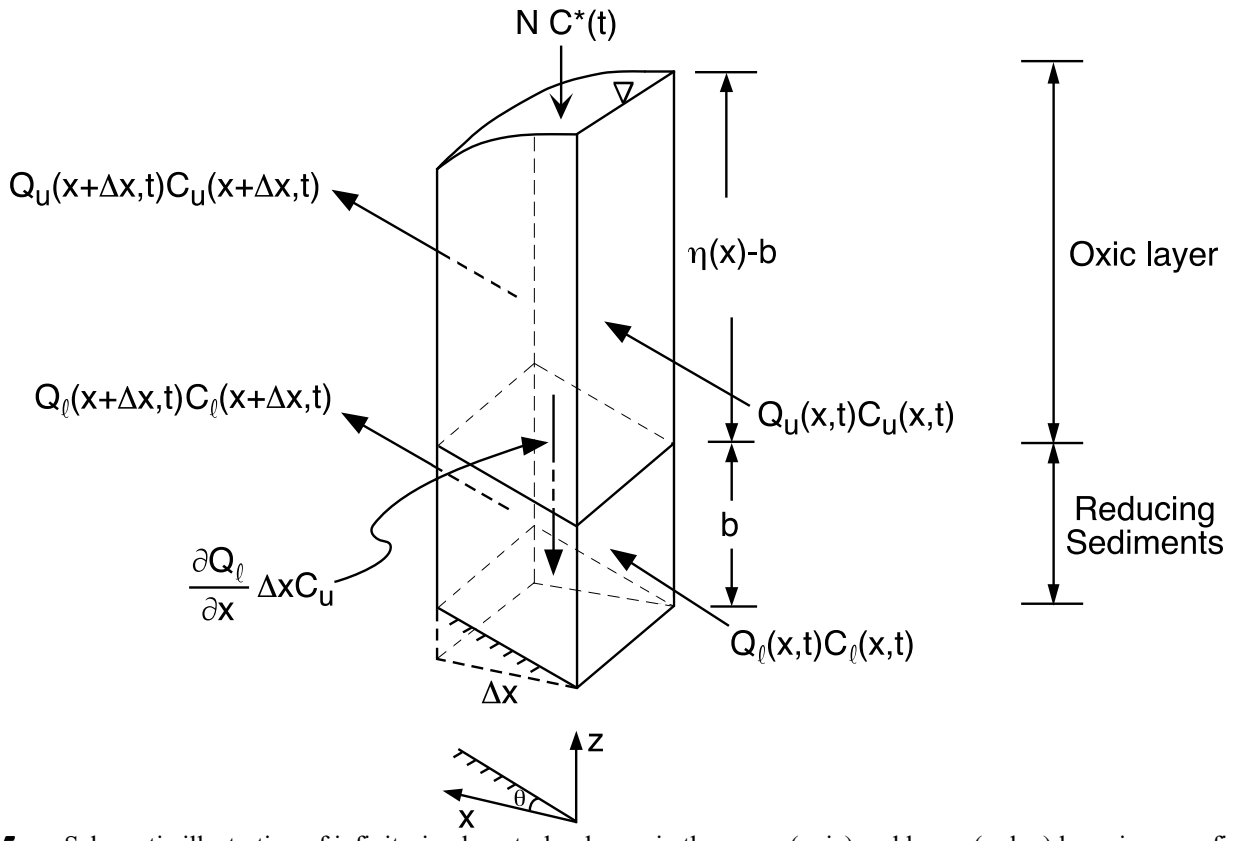

Figure 5. Schematic illustration of infinitesimal control volumes in the upper (oxic) and lower (redox) layer in unconfined aquifer.

$dQ_l/dx = N - dQ_u/dx$ accounts for ground-water flux transfer from the upper layer to the lower layer. After dividing both sides of (18) by $\Delta x\, \Delta t$ and taking the limits $\Delta x, \Delta t \rightarrow 0$, the following partial differential equation is obtained

$$n(\eta - b)\frac{\partial C_u}{\partial t} + \frac{\partial}{\partial x}(Q_u C_u) + \left(\frac{dQ_l}{dx} + n(\eta - b)k_u\right)C_u = N\,C^*(x,t) \tag{17}$$

Equation (17) describes convective-reactive transport of nitrate-nitrogen in the upper layer of the aquifer that is subject to a distributed source of magnitude $C^*(x,t)$, arriving at the water table at a rate equal to the recharge N. In this study, k_u is assumed zero since in oxic waters denitrification is relatively negligible. Equation (17) can be simplified further by expanding the second term and noting that $dQ_T/dx = d/dx\,(Q_u+Q_l) = N$,

$$n(\eta - b)\frac{\partial C_u}{\partial t} + Q_u\frac{\partial C_u}{\partial x} + \left(N + n(\eta - b)k_u\right)C_u = N\,C^*(x,t) \tag{18}$$

2.2.1.2 Lower Layer (Redox Zone)

The application of the mass balance (15) to the lower portion of the control volume in Figure 5, for infinitesimal Δx and Δt, yields

$$\begin{aligned} n\,b\,\Delta x\,C_l(x,t+\Delta t) - n\,b\,\Delta x C_l(x,t) &= Q_l(x)C_l(x,t)\Delta t + \frac{dQ_l}{dx}\Delta x C_u(x,t)\Delta t \\ &- Q_l(x+\Delta x)C_l(x+\Delta x,t)\Delta t - n\,b\,\Delta x\,k_l\,C_l(x,t)\,\Delta t \end{aligned} \tag{19}$$

in which C_l is nitrate concentration in the lower layer [g/m^3], and k_l is a first-order rate loss coefficient [d^{-1}], which accounts for denitrification in the reducing sediments. After dividing both sides of (19) by $\Delta x\, \Delta t$ and applying the limits $\Delta x, \Delta t \rightarrow 0$ to the resulting equation, the governing convection-reaction transport equation for nitrate in the lower layer can be obtained,

$$nb\frac{\partial C_l}{\partial t} + Q_l\frac{\partial C_l}{\partial x} + \left(\frac{dQ_l}{dx} + nbk_l\right)C_l = \frac{dQ_l}{dx}C_u \tag{20}$$

Equations (18) and (20) describe convective-reactive transport of nitrate-nitrogen in the upper and adjacent lower layer of the unconfined aquifer subject to a uniform recharge N and temporally variable nonpoint source of magnitude $C^*(t)$ under steady-state ground-water flow conditions. As mentioned earlier, the solution of Equation (18) is sufficient to describe nitrogen reduction at the base flow if ground waters in the lower layer are assumed to be denitrified entirely (i.e., $k_l = \infty$).

2.2.2 Lagrangian Solution in the Upper Layer

In this section a closed-form solution to (18) is obtained by using asymptotic expansions of the form (7) and adopting a Lagrangian framework. The solution has several advantages. First, it allows, in a rather straightforward manner, the evaluation of the effectiveness of denitrification in riparian zones on nitrogen reduction in base-flow loading to streams. This can be achieved without resorting to complex numerical models that require extensive data, which are either difficult to obtain or costly. Analytical solutions can be used to verify the integrity of complex numerical models. Secondly, the solution is not limited to a particular site; it is rather of a general use given the assumptions. Thirdly, the characteristic Lagrangian solution allows backtracking of unknown historical records based on currently detected pollution levels. The fact that synoptic base-flow loading to streams constitutes a mixture of fairly new and old ages of ground waters makes the solution more suitable for nitrogen source management at the watershed scale. This is because the solution accounts for the average travel time of pollutants originating over the entire transect length of a typical segment in a watershed. It is the average travel time of a given historical record of nitrogen source that is reflected by mixed discharging ground waters at the ground water-surface water interface (i.e., base flow). Therefore, the solution

accounts for the integral effect of nonpoint source in a typical watershed segment (Figs. 3 and 4) on base-flow nitrate-nitrogen loading.

A closed-form solution to (18) can be obtained by dividing both sides of the equation by $Q_u(x)$ and introducing the following Lagrangian-type relationship:

$$\frac{dt}{dx} = n\frac{\eta(x) - b}{Q_u(x)} \tag{21}$$

By recalling the definition of material derivative (convective derivative), Equation (18), after dividing by $Q_u(x)$, can be expressed in the Lagrangian framework as (Appendix B)

$$\frac{dC_u}{dx} + \frac{N + n\,k_u\,(\eta(x) - b)}{Q_u(x)}C_u = \frac{N}{Q_u(x)}C^*[x, t(x))] \tag{22}$$

in which C^* is expressed as an explicit function of x. The solution of (22) is readily obtained in terms of the integration factor,

$$g(x)\,C_u(x) = g(x_0)C_u(x_0) + \int_{x_0}^{x}\frac{N\,C^*[\xi, t(\xi)]}{Q_u(\xi)}g(\xi)d\xi \tag{23}$$

where

$$g(x) = \exp\left\{\int\frac{N + n\,k_u\,(\eta(x) - b)}{Q_u(x)}dx\right\} \tag{24}$$

The evaluation of the integral in (24) is not possible because $\eta(x)$ cannot be expressed explicitly in terms of x. A useful approximation to (23), however, can be obtained for small inclination ($\beta << 1$) by expressing $C_u(x,t)$ in the following asymptotic expansion:

$$C_u(x,t) = \psi_0(x,t) + \psi_1(x,t)\beta + ..., \qquad \beta << 1 \tag{25}$$

in which $\psi_0(x,t)$ and $\psi_1(x,t)$ are functions to be found. The substitution of (7) and (25) into (22), and expanding the coefficients of $C_u(x)$ and C^* in (22), using Taylor series about $\beta = 0$, and collecting terms of equal powers in β, yields the following ordinary differential solutions (Appendix B):

β^0:

$$\frac{d\psi_0}{dx} + \frac{1}{N\,x + Q_0}\left(\frac{N\,\phi_0(x)}{\phi_0(x) - b} + n\,k_u\,\phi_0(x)\right)\psi_0 = \frac{N}{N\,x + Q_0}\frac{\phi_0(x)}{\phi_0(x) - b}C^*[x, t(x)] \tag{26}$$

β^1:

$$\frac{d\psi_1}{dx} + \frac{1}{N\,x + Q_0}\left(\frac{N\,\phi_0(x)}{\phi_0(x) - b} + n\,k_u\,\phi_0(x)\right)\psi_1 = \frac{N}{N\,x + Q_0}\frac{b\,\phi_1(x)}{(\phi_0(x) - b)^2}\left(\psi_0(x) - C^*[x, t(x)]\right) - n\,k_u\frac{\phi_1(x)}{N\,x + Q_0}\psi_0(x) \tag{27}$$

The solutions of (26) and (27) are of the form (23) with the details shown in Appendices (B) and (C):

$$\psi_0(x) = \frac{g(x_0)}{g(x)}\psi_0(x_0) + \int_{x_0}^{x} \frac{N\,C^*[\xi, t(\xi)]}{Q_0 + N\,\xi} \frac{\phi_0(\xi)}{\phi_0(\xi) - b} \frac{g(\xi)}{g(x)} d\xi \tag{28}$$

$$\psi_1(x) = \int_{x_0}^{x} \frac{\phi_1(\xi)}{Q_0 + N\,\xi} \left[\frac{N\,b}{\left(\phi_0(\xi) - b\right)^2} \left(\psi_0(\xi) - C^*[\xi, t(\xi)]\right) - n\,k_u \psi_0(\xi) \right] \frac{g(\xi)}{g(x)} d\xi \tag{29}$$

where

$$g(x) = (Q_0 + N\,x)\left(\sqrt{a^*} - \phi_0(x)\right)^{\frac{b}{2(\sqrt{a^*} - b)}} \cdot \left(\sqrt{a^*} + \phi_0(x)\right)^{\frac{-b}{2(\sqrt{a^*} + b)}} \cdot \left(\phi_0(x) - b\right)^{\frac{-b^2}{a^* - b^2}} \cdot \left(\frac{\sqrt{a^*} - \phi_0(x)}{\sqrt{a^*} + \phi_0(x)} \right)^{n k_u \frac{\sqrt{a^*}}{N}} e^{\left(\frac{n k_u \phi_0(x)}{N}\right)} \tag{30}$$

$$a^* = \eta_l^{\,2} + \frac{(N\,l + Q_0)^2}{K\,N} \tag{31}$$

Equation (21) is also difficult to solve since $\eta(x)$ and $Q_u(x)$ cannot be expressed explicitly in terms of x. An approximate solution is obtained in Appendices B and C by substituting (12) for $Q_u(x)$ in (21) and expanding the right-hand side in Taylor series about $\beta = 0$,

$$t(x) \approx t_0 + \frac{n}{N}\left(\phi_0(x) - \phi_0(x_0)\right) - \frac{n}{2\,N}\sqrt{a^*} \left\{ \ln\left(\frac{\sqrt{a^*} + \phi_0(x)}{\sqrt{a^*} - \phi_0(x)} \right) - \ln\left(\frac{\sqrt{a^*} + \phi_0(x_0)}{\sqrt{a^*} - \phi_0(x_0)} \right) \right\} \tag{32}$$

The solutions (28-32) would have been obtained by direct substitution of the asymptotic approximations (7), (14), and (25) for (x), $Q_u(x)$, and $C_u(x,t)$, respectively, into the partial differential equation (PDE) (18), collecting terms of equal order of powers in β, and then adopting the Lagrangian transformation to the resulting zero- and first-order PDEs.

In Equations (28) and (29), $C^*[\xi\ ,\ t(\xi)]$ implies C^* expressed explicitly in terms of ξ. Thus, if the historical record of C_u is known at spatial point x_0, $C_u(x_0,t_0) = f(t_0)$, then from (25) we deduce that $\psi_0(x_0,t_0) = f(t_0)$ and $\psi_1(x_0,t_0) = 0$, and (25) and (28-32) can be applied to construct future records at any given spatial point x. Conversely, if the current record of C_u is known at spatial point x, $C_u(x,t) = f(t)$, then the historical record at any chosen x_0 in the watershed segment can be reproduced by switching x_0 and t_0 with x and t and using $\psi_0(x,t) = f(t)$. The integrals in (28), (29), and (32) can be evaluated numerically; e.g., using the Romberg method, or using any readily available computer software (e.g., Mathcad, Mathematica, etc.).

It should be noted that $t(x)$ in (32) can be interpreted as the average age of ground waters discharging at spatial point x, which originate at time t_0 between x_0 and x. We note that it is not only a function of the ground-water flow rate at upstream boundary of the ground-watershed, but also the geometric and hydraulic properties of the aquifer and the recharge rate. Thus, Equation (28) indicates that a mixture of newly-recharged and old aged waters originating over transect length l affects the quality of current discharges to a stream, with the impact of aquifer bed inclination approximated by Equation (29).

3. Potential Nitrate Reduction by Deep Denitrification

In this section we demonstrate the effectiveness of denitrification in the subsurface on potential nitrogen reduction in riparian buffer zones. The methodology is applied to paired agricultural watersheds in the mid-Atlantic coastal plain, and the site of study is hereafter referred to as the Locust Grove (Figure 1).

3.1 Study Site Description

3.1.1 General

Figure 6(a) shows the portion of the Locust Grove study site (378 km^2) in Kent County, Maryland, which is targeted for new drilling activities and measurements of water levels and stream discharges by the USGS (Baltimore and Dover). The site is composed of two agricultural watersheds of areas that are drained by the Morgan Creek and the Chesterville Branch (Figure 1). This site is bounded from the north by the Sassafras River. Both streams drain in to the Chester River, which borders Kent County in the south and is located along the northeastern shore of the Chesapeake Bay. Agriculture dominates the landscape in the study area and most of the land there is used to grow corn and soybeans in an annual rotation with winter wheat. Riparian forested areas are marginal and restricted to strips along the two creeks and a part of the land is used to grow ornamental trees. Soil in the study area is predominantly silt loam and to a lesser extent ranges from loam to sandy and gravelly loam. The area is underlain by the surficial (Columbia) aquifer, which consists of sand and gravel of fluvial origin.

Figure 10(a) shows regressed record of nitrate NO_3^- (mg/L) loading from fertilizers to the water table starting in the year 1940 (adapted from *Böhlke and Denver*, 1995). The data are based on annual N load from fertilizers estimated from fertilizer use records of the U.S. Department of Agriculture from 1945-1985 (*Alexander and Smith*, 1990) and from records of the U.S. Environmental Protection Agency for 1985-1991. The data, however, are regionally averaged by apportioning the annual tonnage for the state of Maryland according to the fraction of the fertilized acreage within Kent County (1945-1985) or the fraction of the state expenditures attributed to Kent County (1985-1991). The estimate of annual application of N in fertilizer was estimated to be around 12 $g/m^2/yr$, and an independent estimate by *Donigian et al.* (1991) indicated a value of 9 $g/m^2/yr$ for the Chester River watershed.

3.1.2 Geology of the Area

Geologic units in Locust Grove, and in Kent County, in general are chiefly composed of southeast-dipping Coastal Plain sediments that form wedge-shaped sedimentary packages that thicken to the southeast. Truncating and blanketing the top of these units are coarse sediments of dominantly fluvial origin (*Bachman*, 1984; *Drummond*, 1998). From

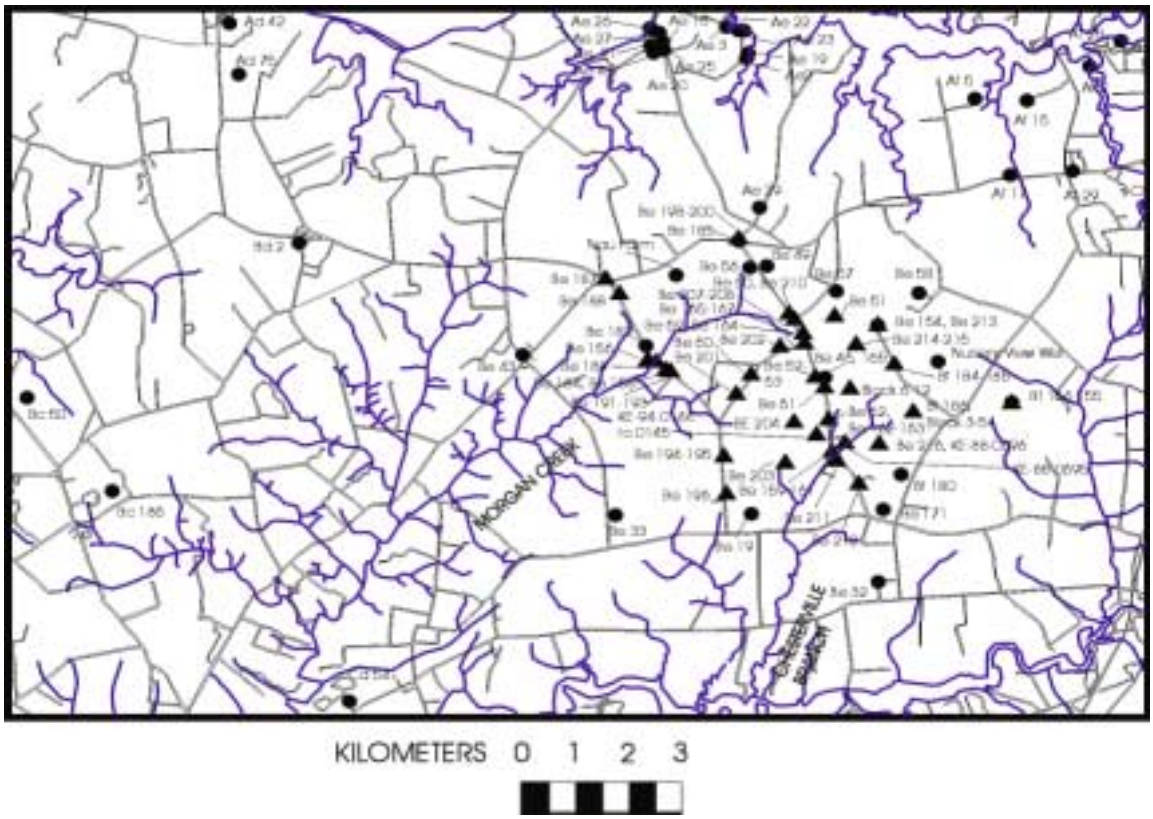

Figure 6. Wells network in the study area. A triangle refers to a well from which the USGS synoptic ground-water levels and quality are measured, and a solid circle refers to a core hole location.

youngest to oldest, the geologic formations in the Locust Grove area and their regional or correlatable equivalents are (following *Hansen*, 1992): The Upper Miocene (?) to Lower Pliocene (?) Pensauken Formation (equivalent to the Wicomico and Columbia Formations), Middle to Upper Oligocene Old Church (?) Formation, Upper Paleocene Aquia Formation, Lower Paleocene Hornerstown Formation, Upper Cretaceous Severn Formation (part of the Monmouth Group), Upper Cretaceous Mt. Laurel Formation (part of the Monmouth Group) and the Upper Cretaceous Matawan Group. Lithologic descriptions that follow are based on the work by *Hansen* (1992) on core hole Ken Bf 180 near Chesterville in Kent County. Some additional description is based on personal communication from *Dave Krantz* (USGS-Dover, 1999) based on drilling in the Locust Grove area. A description for each formation is given in Appendix E.

3.1.3 Hydrostratigraphy

In the Locust Grove site and adjoining areas, the Pensauken Formation, Aquia Formation, and equivalents to the Columbia aquifer comprise the surficial unconfined aquifer in the area. Underlying the surficial aquifer is the first aquitard or confining unit composed of the units of the Aquia Confining Layer, although areal or regional continuity of this unit is uncertain. Note that for regional studies, some investigators group the Aquia and the underlying Hornerstown together to form the Aquia Formation (*Clark*, 1915; *Overbeck and Slaughter*, 1958). *Drummond* (1998) grouped sediments including the Pensauken Formation and Kent Island Formation to form the uppermost Columbia aquifer. He next defined, for his MODFLOW model of Kent County, a lower aquifer, the Aquia, comprised of the Old Church, Nanjemoy, Aquia and Hornerstown Formations, as done by *Hansen* (1992). The latter noted that the Columbia aquifer in Kent County (composed chiefly of the Pensauken Formation), is hydraulically connected to the subcropping Aquia aquifer locally in Locust Grove. Regionally, the Aquia aquifer includes the lowermost Hornerstown Formation (*Overbeck and Slaughter*, 1958; *Hansen*, 1992; *Drummond*, 1998), but *Böhlke and Denver* (1995) and *Krantz* (1998, personal communication) have cited the large gamma spike at the base of the Aquia Formation, above the Hornerstown Formation, as a confining layer locally. However, *Hansen* (1992) has cited the Severn Formation and basal beds of the Hornerstown as a confining unit underlying the Aquia aquifer regionally. The finer-grained nature of the Severn Formation is a definite factor in establishing this unit as the main, or part of the main, confining unit beneath the Aquia aquifer.

Overbeck and Slaughter (1958) and *Drummond* (1998) classified the Monmouth aquifer as composed of the Mt. Laurel Formation and sandy units of the Matawan Formation. Beneath the Monmouth aquifer, the Matawan is a well defined confining unit in the area (*Overbeck and Slaughter,* 1958; *Hansen*,1992; *Drummond*, 1998).

Krantz (personal communication 1998, 1999) identified local hydrostratigraphic units in the Locust Grove area based on gamma and lithologic logs from a recently established well network shown in Figure 7. From top to bottom, these are: Pensauken Formation (which is the Columbia aquifer in Kent county), Aquia sands, redox zone, Aquia confining layer tight (impermeable) unit, Hornerstown, Hornerstown sand (?), Hornerstown confining layer, and Severn. The Aquia confining layer has been identified and documented as the gamma spike also observed in the report by *Hansen* (1992) for KE Bf 180.

For the Aquia confining units, *Krantz* (personal communication 1998, 1999) characterized the Aquia redox zone as a low-permeability oxidized unit. Beneath this is a clayey unit, which gives a tight gamma spike in geophysical logs, comprising the Aquia impermeable confining layer. Based on the averages of 8 thicknesses measured for the Aquia redox confining layer and 10 thickness measurements for the tight Aquia confining layer, average thicknesses of 4.2 meters and 3.8 meters were calculated for the redox layer and tight (impermeable) layer, respectively.

3.1.4 Locust Grove Local Well Network and USGS-USEPA Data Sets (1997-1999)

A recent set of wells and core holes was established in the Locust Grove site based on an EPA-USGS Interagency Agreement on Ecosystem Restoration in the Chester River watershed. Figure 6 shows wells network and core holes locations provided by *Drummond* (1997) of the Maryland Geological Survey and *David Krantz* (1998-1999) of the USGS-Dover. The wells network is used for measuring ground-water levels in wet and dry seasons, collecting ground-water samples for geochemical analysis, and obtaining core samples for the description of the hydrostratigraphy. In Appendix F, Table 1 lists core holes either recently drilled by the USGS in Locust Grove or obtained from records with information on what geologic information was provided as of this writing. Table 2 in Appendix F provides some recent synoptic water table measurements provided by the USGS for Locust Grove.

3.2 Preliminary Assessment

Figure 7 (b) is an enlargement to the local area contained within the dashed box in Figure 7 (a). Figure 7(c) shows cross section A-A', which is synthesized from a three-dimensional geologic model developed from the core holes (Table 2) obtained from *D.Drummond* (Maryland Geological Survey) and *D. Krantz* (U.S. Geological Survey, Dover), and using the GMS module (The Department of Defense Ground-water Modeling System). The cross section runs from the northeastern branch of the Morgan Creek to the northwestern branch of the Chesterville Branch. The cross section, which spans the surficial Columbia-Aquia aquifer, is chosen for the assessment of impacts of the geohydrology and geochemistry on reductions of NO_3^- loading to the Morgan Creek and the Chesterville Branch. In particular, we focus on the integral effect of the zone of reducing sediments and regional dip of the stratum on the reduction of input nitrogen that is recharging the water table. Because oxic waters dominate in the upper layer, denitrification of NO_3^- is assumed to occur exclusively in the lower layer of reducing sediments and at an instantaneous rate; i.e., $k_1 = \infty$ and $C_1(x,t) = 0$. Thus, NO_3^- concentration C(x,t) is therefore given by:

$$C(x,t) = \frac{Q_u(x)\,C_u(x,t)}{Q_T(x)} \tag{33}$$

where $C_u(x,t) \approx \psi_0(x,t) + \beta\,\psi_1(x,t)$ and $Q_T(x)$ and $Q_u(x)$ are given by (10) and (14). At the base flow in the Morgan Creek and the Chesterville Branch, we simply evaluate $C(l,t)$, and l, recall, is the distance from the water divide to the stream (Figures 3 and 4).

Figures 8(a) and 9(a) compare theoretical head of Equations (4) and (7) with average annual measured heads at the Morgan Creek and Chesterville Branch sides of the Cross Section A-A' shown in Figure 7(c), respectively. The inclination of the surficial Columbia-Aquia aquifer bed at this particular cross section was $\beta = 0.0052$ (0.3°), which is obtained from the constructed geologic model. *Böhlke and Denver* (1995) reported a value of about 0.4° for the regional dip. The fitted recharge value for the Morgan Creek side of cross section A-A' and the conductance K'/b' were

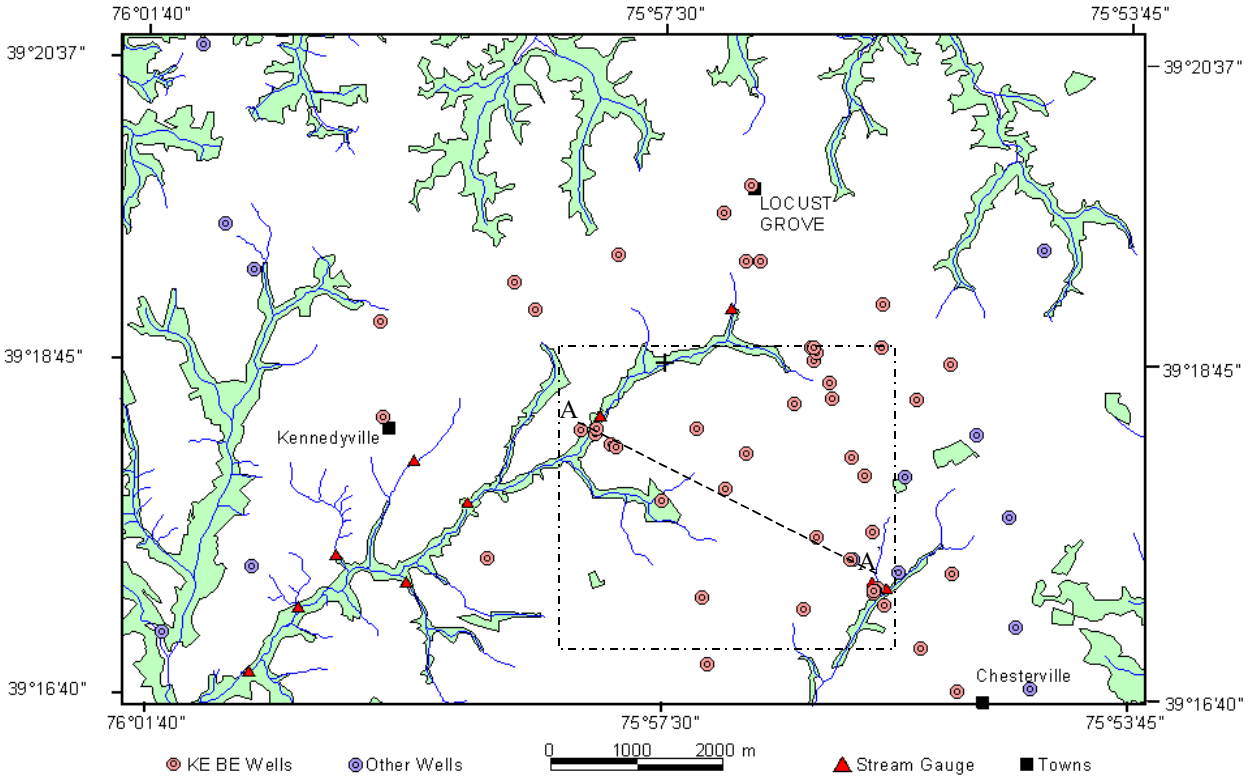

Figure 7(a). Overview of the location of cross section A-A' relative to the Locust Grove site and the wells network.

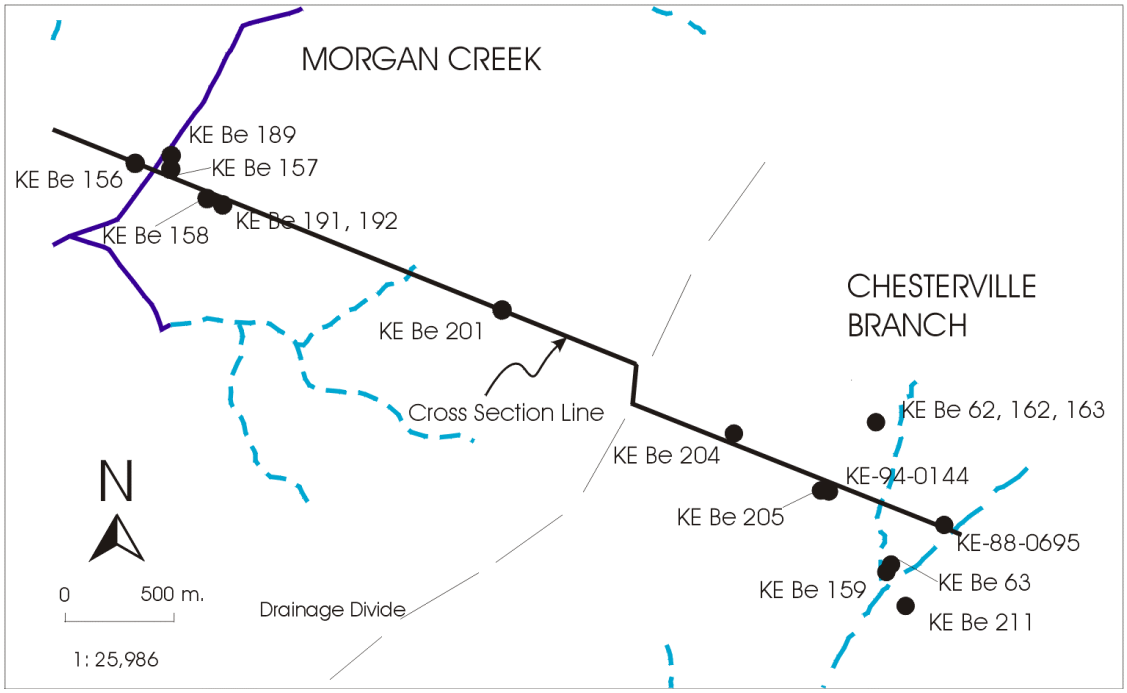

Figure 7(b). Cross section A-A' between the Morgan Creek and the Chesterville Branch with adjacent wells labeled. The dashed line delineates the ground-water divide.

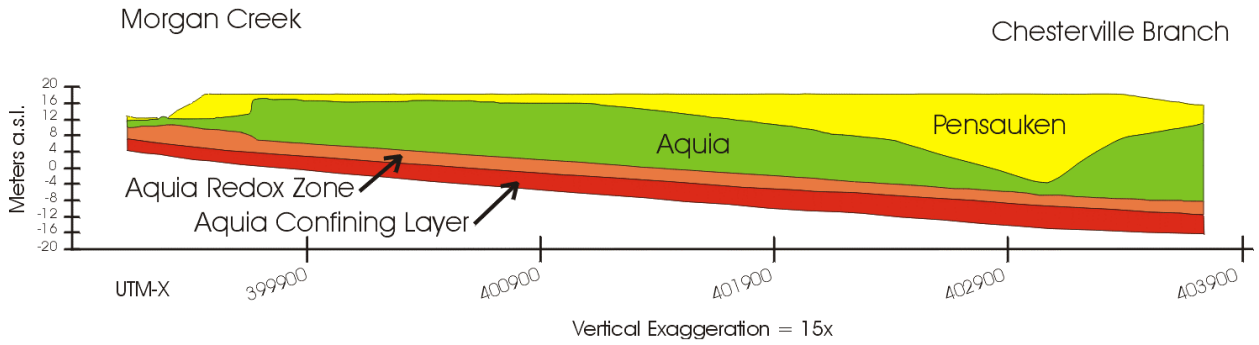

Figure 7(c). Hydrostratigraphy along cross section A-A' illustrating the relative position of the redox zone.

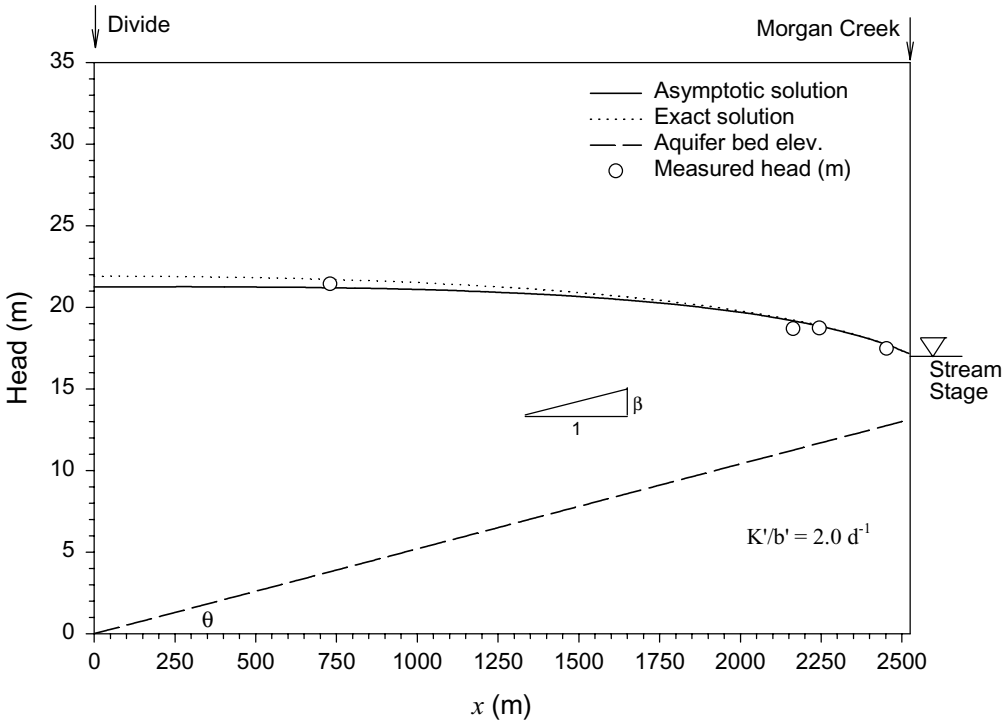

Figure 8(a). Measured versus estimated heads at Morgan Creek watershed.

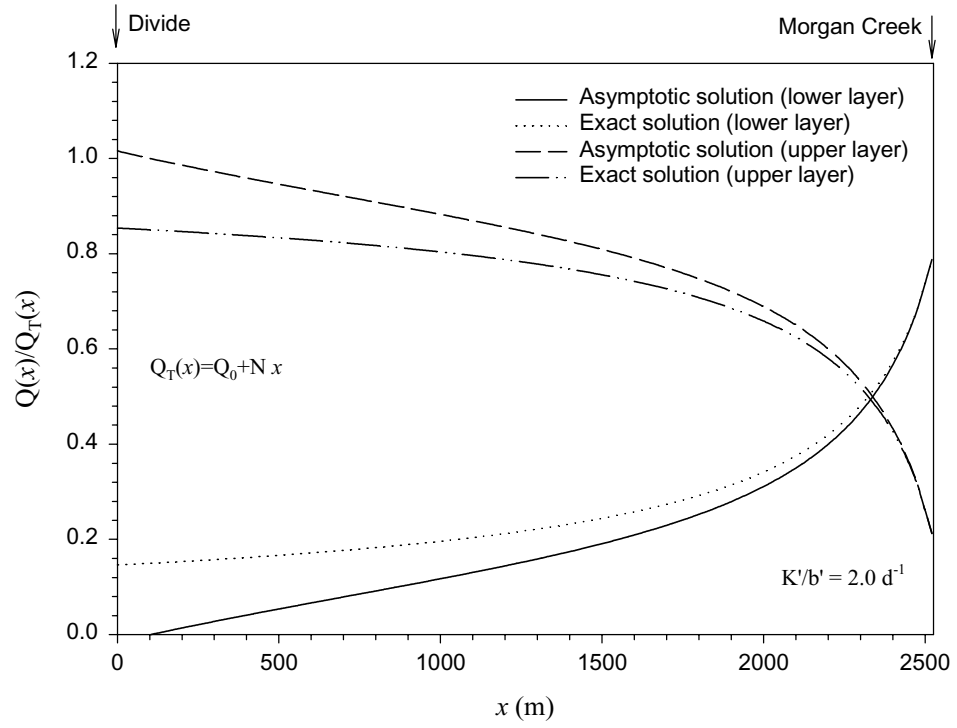

Figure 8(b). Measured versus estimated ground-water fluxes at Morgan Creek watershed.

2.4×10^{-4} m/d (3.5 in/yr) and 2.0 d^{-1}, respectively, whereas at the Chesterville Branch, calibration yielded $N = 2 \times 10^{-3}$ m/d (29 in/yr) and $K'/b' = 2.0\ d^{-1}$. However, an independent estimate of $K'/b' = 0.2\ d^{-1}$ ($K' = 0.4$ ft/d, $b' = 2$ ft) was obtained by *Drummond* (1998) by calibrating a regional ground-water model (MODFLOW) for Kent County. An independent value for the hydraulic conductivity of magnitude 16.76 m/d is used. This value has been suggested by *Reilly et al.* (1994) for the surficial aquifer and within the range of values reported by *Drummond* (1998). The calibrated recharge at Morgan Creek was somewhat low, however, it is consistent with the relatively poorly-drained soils at the Morgan Creek watershed (Hydrologic Classes C and D). In general, recharge to the northern Atlantic Coastal Plain aquifer system has been estimated to range from 10 to 25 in/yr (*Meisler*, 1986), and the average of the above fitted values is about 16 in/yr, which is within range. Although the calibrated values may be valid locally (i.e., to the particular cross section), they may not be generalized to the entire area of the paired watersheds. The exact head distribution of Equation 4 and the asymptotic approximation of Equation 7 compared very well as Figures 8(a) and 9(a) show. Figures 8(b) and 9(b) compare ground-water flux in the upper (oxic) layer and lower (anoxic) layer, in both creeks, using exact solutions (Equations 11 and 12) and approximate expansions (Equations 13 and 14). The thickness of the lower layer of reducing sediments (redox zone) was estimated to be 3.2 m on the basis of the three-dimensional geologic model (see, Figure 6(c)). At Morgan Creek, about 80% of the total recharge was discharged from the redox zone (lower layer), and the remaining 20% was discharged from the upper layer. Thus, most of the ground waters entered the reducing sediments because of the positive inclination of aquifer bed ($\beta = 0.0052$) toward the Morgan Creek. At the Chesterville Branch, however, more than 80% of the base flow was discharged from the upper layer (i.e., all discharge ground waters escaped denitrification), because of negative inclination relative to the reference ($\beta = -0.0052$ in Figure 4).

Although the exact head solution and the approximate one compared very well, that was not the case for the ground-water fluxes in Morgan Creek as Figure 8(b) indicates. The approximate (asymptotic) solution overestimated the flux in the upper layer, especially toward the drainage divide, by as much as 16% and, consequently, the ground-water flux in the lower layer was underestimated by the same amount. The error, however, declines toward the discharging point (i.e., the creek) where an almost exact estimate of the base flows is achieved by the asymptotic solution. The estimates of ground-water fluxes in the Chesterville Branch side were almost similar between the exact and asymptotic solutions (Figure 9(b)).

Figures 10(a-d) and 11(a-d) show the impact of the historical record (1940-1992) of the recharging nitrate levels $C^*(t)$ in Figure 10(a) on the base-flow nitrate-nitrogen levels at Morgan Creek and Chesterville Branch, respectively. We have assumed that the average nitrate concentrations at the recharging waters C^* after year 92 remained constant at 17 mg/L. The breakthrough values in the figures are obtained from Equations (21), (28-32) and (33) and assuming ground waters are instantly and entirely denitrified in the lower layer (redox zone or layer of reducing sediments). In the estimations, we used $x_0 = 50$ m, $t_0 = [0, 52]$, and $C_u(x_0,t_0)$ in Figure 10(a) was derived by assuming complete mixing of nitrate-N in ground waters between the water divide (at $x = 0$) and $x_0 = 50$ m. The assumption of complete mixing from $x = 0$ to 50 m is valid, considering the distances from the water divide (Figure 7a) to both creeks ($\mathbf{l} = 1112$ m and 2521 m for the Chesterville Branch and the Morgan Creek, respectively).

Figure 10(b) shows NO_3^- discharged at Morgan Creek: mass flux relative to the steady-state total nitrate input over the entire transect $\mathbf{l} = 2521$ m (N L $C^*(\infty)$, $C^*(\infty)$ is the assumed steady value of 17 mg/L). The predicted future synoptic corresponds to the record shown in Figure 10(a), and because of relatively low recharge of 0.00024 m/d, its impact may not be felt at Morgan Creek before year 2092. That is, at year 2092, the mixed-discharging waters at the Creek will consist of very old ground waters, which were recharged at year 1940, as well as newer ground waters, including those that would be recharging at the immediate neighborhood (e.g., in riparian zones). According to the definition of t(x) in Equation (29), the average age of ground waters that would be discharged from the upper layer at Morgan Creek at year 2092 is 152 years, being originated as recharging waters over a distance of 2521 m between the Creek and the water divide. In order to predict the base-flow loading pre year 2092, the input record pre year 1940 will be needed. Equivalently, base-flow nitrate levels pre year 2092 are impacted by nitrate levels in recharging ground waters before year 1940.

The impact of denitrification in the reducing sediments and the aquifer bed inclination is evident in Figure 10(b). For a positive dip angle of 0.3°, there is a potential for 80% reduction of NO_3^- at the base flow, provided that ground waters entering the redox zone are entirely denitrified. A steady state concentration of NO_3^- of 3.4 mg/L (0.2×17 mg/L) compared to 17 mg/L at the source is predicted at the discharge in Morgan Creek. Because of the nature of the dip (Figure 7 (c)), more than 80% of ground waters were predicted to discharge to the Chesterville Branch through the upper layer (Figure 11(a)), therefore avoiding potential denitrification in the lower layer (redox zone) and resulting in much less reductions of NO_3^- levels by 15% at a steady concentration of NO_3^- of about 15 mg/L at the base flow at

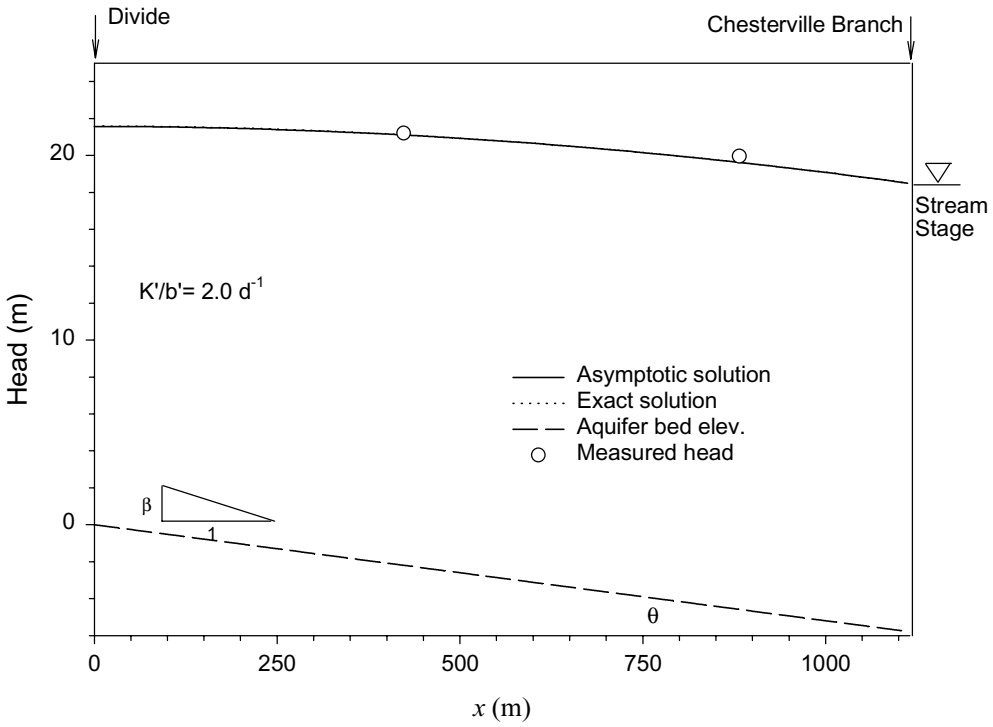

Figure 9(a). Measured versus estimated heads at Chesterville Branch watershed.

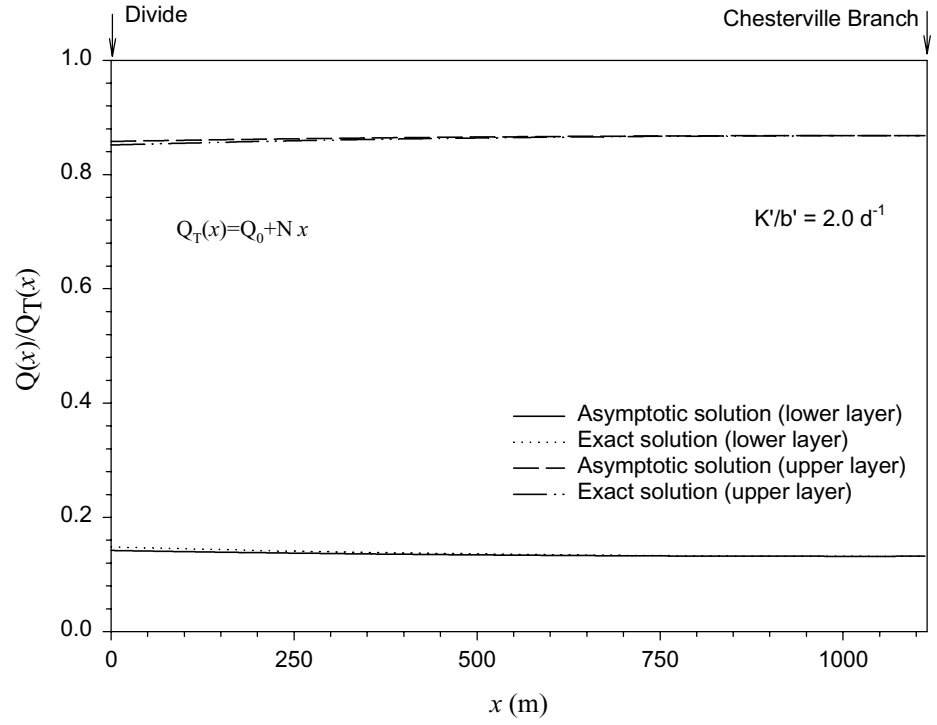

Figure 9(b). Measured versus estimated ground-water fluxes at Chesterville Branch watershed.

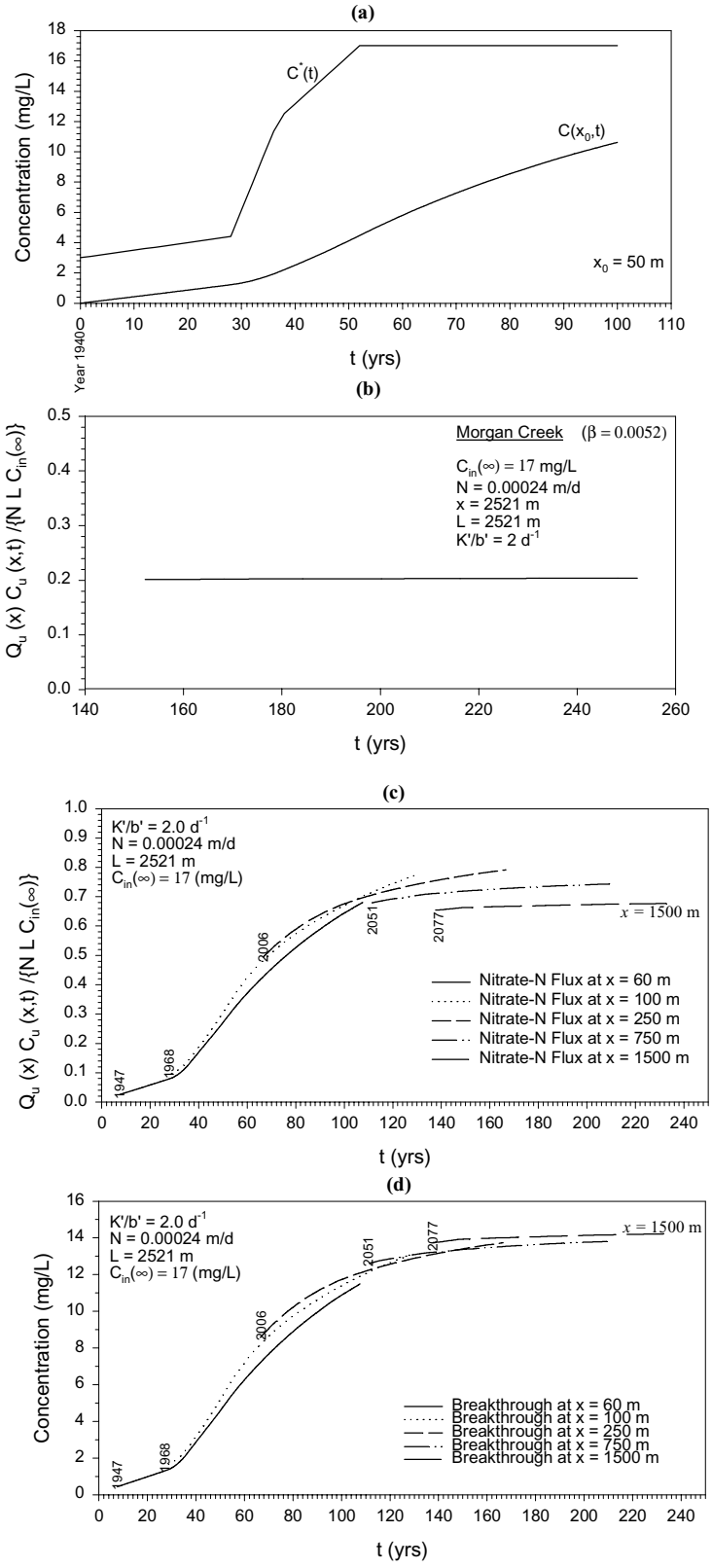

Figure 10. (a) Historical variations of NO_3^- concentration at the recharge (at the water table) and at x_0 = 50 m in the upper layer, (b) Mass flux of NO_3^- in time at the discharge to Morgan Creek relative to steady-state input, (c) Mass flux of NO_3^- discharged from upper layer to Morgan Creek relative to steady-state input versus time, and (d) NO_3^- concentration versus time.

Chesterville Branch (Figure 11(c)). The less effective capacity of the subsurface sediments to reduce NO_3^- at the Chesterville Branch is not only influenced by relative position of the redox zone (i.e., negative β) but also by the relatively higher recharge rate.

It is clear from Figure 11(c) that the impact of the historical nitrate input (Figure 11(a)) at the recharging waters appeared earlier at the Chesterville Branch at year 1979 because of the relatively greater recharge and smaller travel distance from the water divide. Thus, ground waters discharging to the Chesterville Branch are relatively younger when compared to the discharging waters at Morgan Creek and, therefore, their relatively greater NO_3^- concentrations are also the result of more recent and greater nitrate loading at the source. In order to show clearly the impact of historical input variations ($C^*(t)$), we considered the hypothetical case of positive inclination (0.3^o, $\beta = 0.0052$) to be applicable to the Chesterville Branch (i.e., the redox layer becomes increasingly shallower toward the Chesterville Branch). Figure 11(b) shows that a reduction of 30% is incurred due to deep denitrification, whereas 80% reduction was predicted for the same, but actual, scenario at Morgan Creek. This may be explained on the basis that expected reductions by denitrification are offset by elevated levels of NO_3^- in fairly younger discharging ground waters due to the historical input variations.

Böhlke and Denver (1995) reported values of zero mg/L of NO_3^- at the discharge at Morgan Creek and 3-5 mg/L at the Chesterville Branch, and the location where these values were measured within close range to cross section A-A'. Our predictions, based on the theoretical framework, were 3.4 mg/L and 15 mg/L at Morgan Creek and the Chesterville Branch, respectively. The overly predicted NO_3^- levels at the Chesterville Branch may be the result of ignoring the impact of riparian woodlands as natural filters, where ground waters discharging from the oxic upper layer may be denitrified in silty, peat-rich stream valley sediments. Recall, in the analysis we assumed that $k_u = 0$. The case where NO_3^- removal occurs in the riparian stream valley will be addressed in a future effort. The preliminary analysis is consistent with the geochemical analysis and the results reported by *Böhlke and Denver* (1995) with respect to the behavior of nitrate-nitrogen in ground water in the paired watersheds. It appears that a combination of deep denitrification and historical input variations seem to impact the quality of ground waters being discharged to Morgan Creek and the Chesterville Branch. The capacity of deep denitrification to reduce NO_3^- discharge to streams is dependent on the size of the drainage area as well as the relative position of the redox zone to the surface.

3.3 Removal Capacity

A simple relationship can be developed, which measures the efficiency for nitrate reduction in ground-water sheds. The removal capacity index I is based on the following assumptions: 1) ground-water recharge, including boundary fluxes, is at steady state (e.g., annual average) and drained entirely by a stream; 2) steady-state nitrate concentrations in ground water on the assumption that current agricultural practices would persist at the current steady levels of net nitrate-nitrogen input, C^*, to ground water; and 3) complete mixing in each of the modeled zones. We define the removal capacity index as the ratio of the rate at which the constituent is lost out of the system to the rate of input, at steady state,

$$I_{RC} = \frac{\left[N\ell\overline{C}^* + Q_0C_0\right] - \left[Q_u(\ell)C_u\ell + Q_l(\ell)C_l(\ell)\right]}{N\ell\overline{C}^* + Q_0C_0} \tag{33}$$

where $\overline{C^*} = (1/l)\int_0^l C^*(x)\,dx$. If we assume that nitrate input persists at the current level of C^* and that steady and uniform concentrations in ground water are achieved, and integrate (17) from $x = 0$ to $x = l$ after dropping the term with partial derivative in time, we have

$$\int_0^l \frac{\partial}{\partial x}(Q_u(x)\,C_u(x))\,dx + \int_0^l \left(\frac{dQ_l(x)}{dx} + n_u\,(\eta - b)\,k_u\right) C_u(x)\,dx = \int_0^x N\,C^*(x)\,dx \tag{34}$$

thus,

$$Q_u(l)\,C_u(l) - Q_u(0)\,C_0 + (Q_l(l) - Q_l(0))\,\overline{C_u} + n_u\,k_u\,\overline{(\eta - b)}\,\overline{C_u}\,l = N\,\overline{C^*}\,l \tag{35}$$

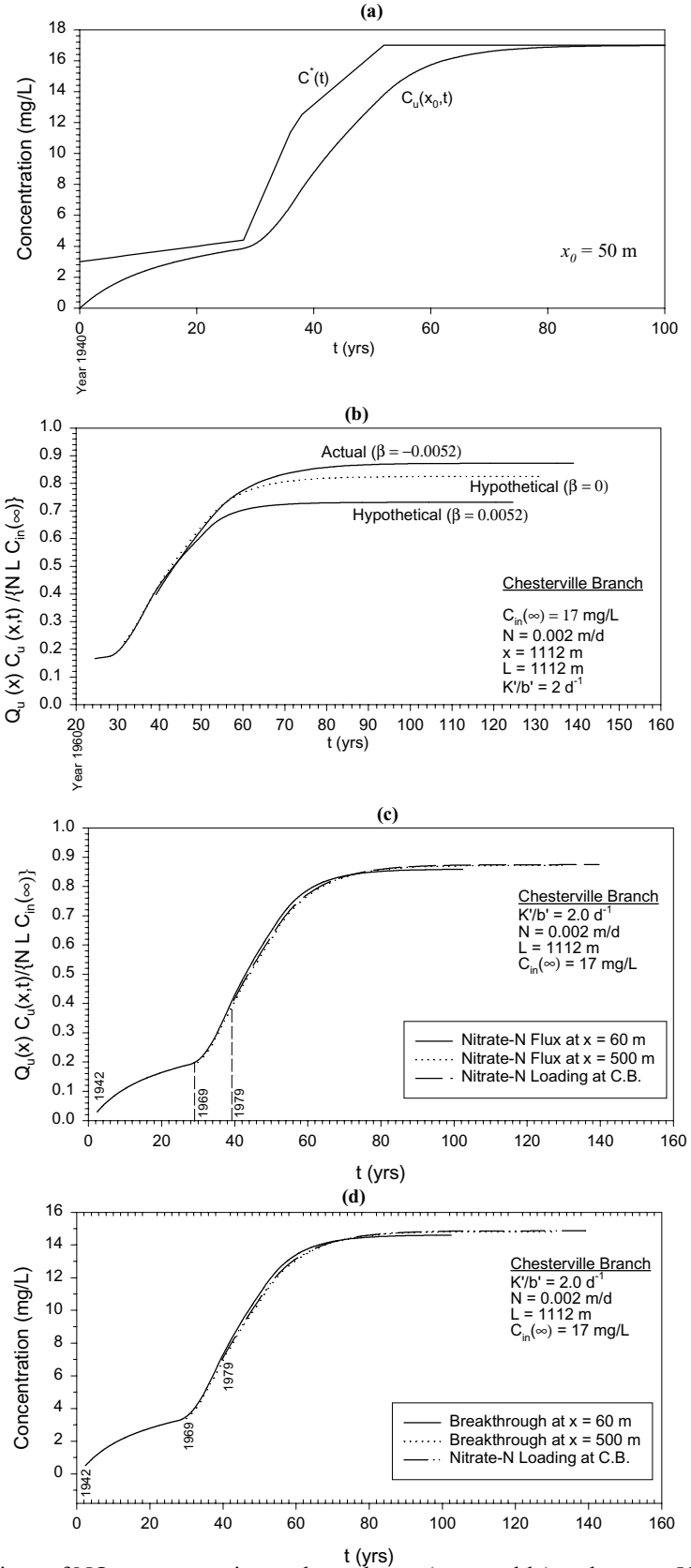

Figure 11. (a) Historical variations of NO_3^- concentration at the recharge (water table) and at x_0 = 50 m in upper layer, and (b) Mass flux of NO_3^- in time at the discharge to Chesterville Branch relative to steady-state input, (c) Mass flux of NO_3^- discharged from upper layer to Chesterville Branch relative to steady-state input versus time, and (d) NO_3^- concentration versus time**.**

where $\overline{C_u} = (1/l)\int_0^l C_u(x)\,dx$; $\overline{C_l} = (1/l)\int_0^l C_l(x)\,dx$; and $\overline{(\eta - b)} = (1/l)\int_0^l (\eta(x) - b)\,dx$ is the average thickness of flow in the upper (oxic) layer. By making use of the third assumption, we have $C_u(l) = \overline{C_u}$, which upon the substitution into (35) yields

$$C_u(l) = \frac{N\,\overline{C^*}\,l + (1 - (b/\eta_0))\,Q_0 C_0}{Nl + (1 - (b/\eta_0))\,Q_0 + n_u\,k_u l\,(\overline{\eta(x) - b})} \tag{36}$$

in which $\eta_0 = \eta(0)$ is the water-table elevation relative to the aquifer bed at the inlet boundary; n_u is the porosity of the oxic layer; and as shown in Appendix D,

$$\overline{\eta(x) - b} = -\frac{1}{\beta}\left\{\frac{1}{K}\left(\frac{N\,l}{2} + Q_0\right) + \frac{\eta_l^{\,2} - \eta_0^{\,2}}{2\,l}\right\} - b \tag{37}$$

In (36) we made use of (11) and (12). Similarly, we integrate Equation (20) from $x = 0$ to $x = l$:

$$Q_l(l)\,C_l(l) - Q_l(0)\,C_0 + n_l\,k_l\,\overline{C_l}\,l = \left(Q_l(l) - Q_l(0)\right)\overline{C_u} \tag{38}$$

The use of the third stated assumption ($C_l(l) = \overline{C_l}$, $C_u(l) = \overline{C_u}$) and the substitution of (11) for $Q_l(0)$ and $Q_l(l)$, leads to

$$C_l(l) = \frac{(b/\eta_0)\,Q_0 C_0 + \left((b/\eta_l)(Nl + Q_0) - (b/\eta_0)\,Q_0\right)C_u(l)}{(b/\eta_l)(N\,l + Q_0) + n_l b\,k_l l} \tag{39}$$

in which n_l is the porosity of the redox layer. Finally, we obtain the following form for the removal capacity index I_{RC} given by (33) for the case of a water divide at $x = 0$; i.e., $Q_u(0) = Q_l(0) = 0$,

$$I_{RC} = 1 - \frac{1 + n_l\left(k_l/N\right)\left(\eta_l - b\right)}{\left[1 + n_u\left(k_u/N\right)\left(\overline{\eta(x) - b}\right)\right]\left[1 + n_l\left(k_l/N\right)\eta_l\right]} \tag{40}$$

in which I_{RC} may be used as a measure for the removal efficiency of NO_3^- in an agricultural catchment. If h_l = b and assuming that ground waters are instantly denitrified in the redox layer ($k_l \to \infty$), we have I_{RC} =1; because the aquifer below the stream would be entirely occupied by the redox layer where all ground waters would be intercepted by the reducing sediments before discharging to the stream. In this particular case, the redox zone acts as a potential natural filter for the entire subwatershed, which is not uncommon to the northeastern branch of Morgan Creek where the streambed is almost underlain by the redox zone at several locations as the constructed geologic model predicted. If k_u = 0 and $k_l \to \infty$, we have $I_{RC} = b / \eta_l$, which is the case assumed in the application in the previous section where nitrate reduction is entirely controlled by aquifer geometry at the discharging points. Figure 12 shows the variation of I_{RC} with **l** for different values of the dimensionless parameter $\varepsilon = N/\left\{(K'/b')W\right\}$. The removal capacity decreases with transect length, **l**, and increases with decreasing ε. This relationship shows that NO_3^- removal is also influenced by the characteristics of groundwater-surface-water interface and the recharge rate. The greater the recharge, or equivalently, the smaller the streambed hydraulic conductance and width, the smaller the removal efficiency.

Figure 13 illustrates possible nitrate loss pathways in a riparian zone and related hydrologic and hydrogeologic factors. In a stream riparian environment, the flux Q_0 at $x = 0$, which is equal to the total drainage from the agricultural uplands of the watershed, may be much greater than the recharge N; i.e., N ≈ 0. Also, nitrate loading is dominated by drainage from agricultural uplands, $Q_0\,C_0$, as opposed to input from riparian zones, where N C^* may be relatively ignored. Thus, Equation (33) can be used to derive an expression for the removal capacity for nitrate introduced at the upgradient boundary of the riparian zone at $x = 0$, by setting N = 0 in (36) and (39), and substituting the resulting expressions into (33):

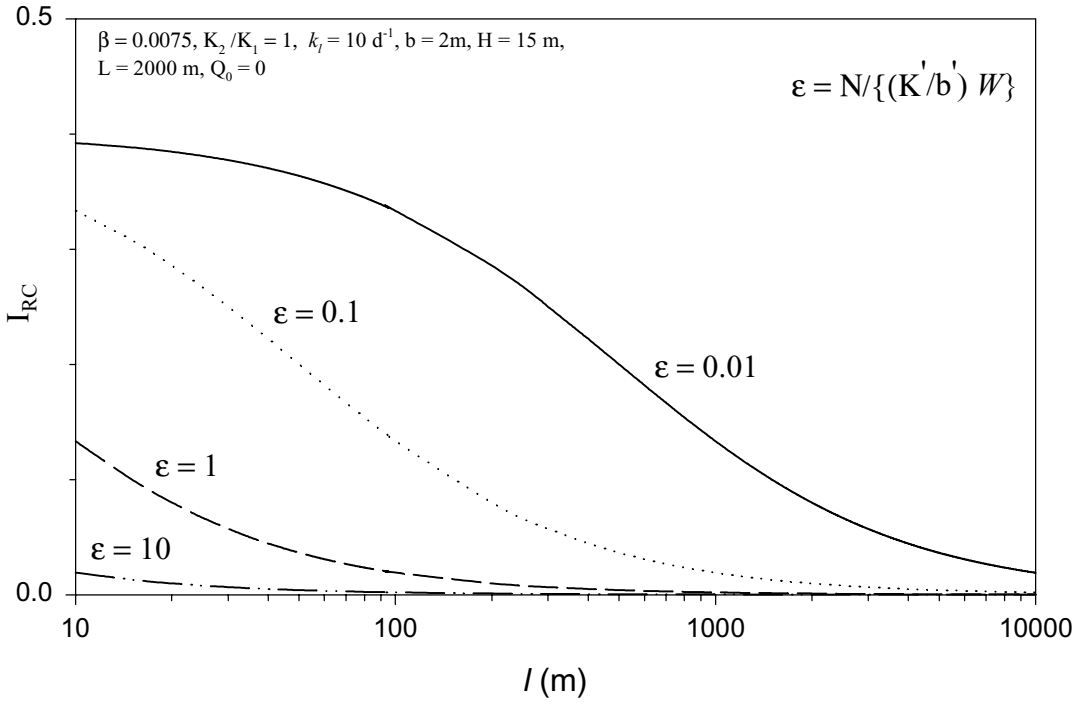

Figure 12. Semi-log plot of the removal-capacity index I_{RC} versus **l** for different values of the dimensionless parameter ε.

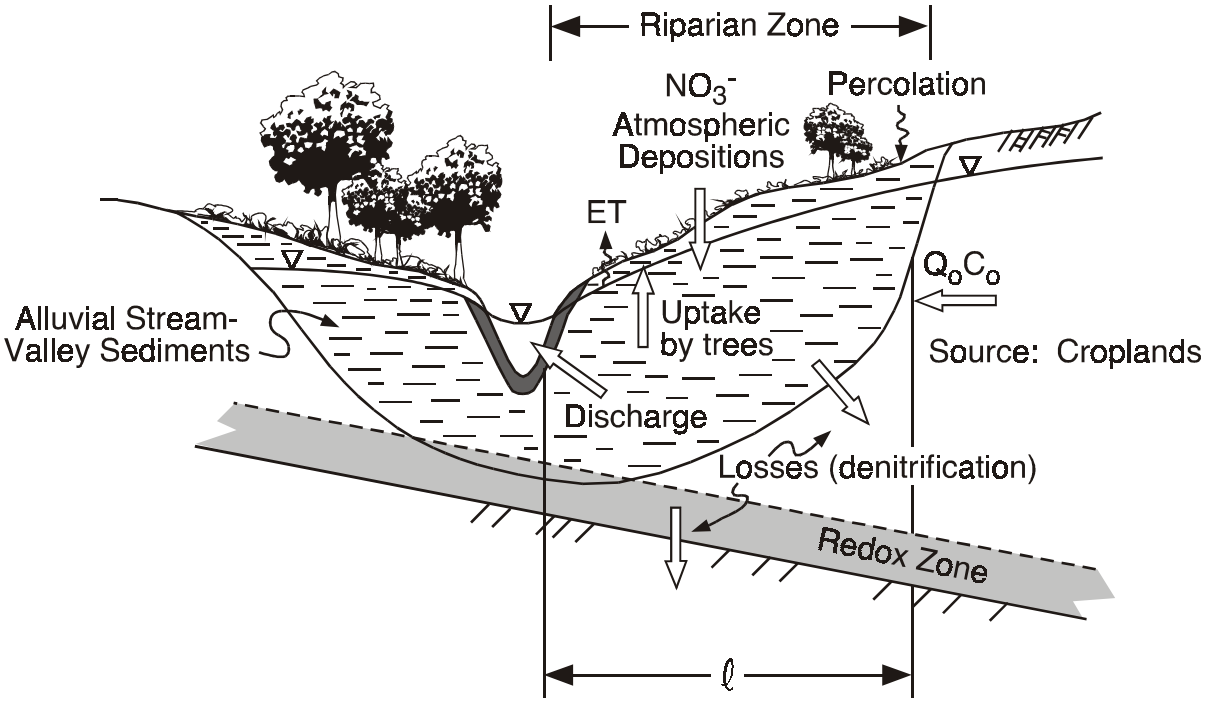

Figure 13. Illustration of a riparian zone showing potential NO_3^- loss pathways in organic-rich soils and subsurface sediments and related hydrological factors.

$$I_{RC} = 1 - \frac{1}{1 + (n_u k_u \eta_0 \, l/Q_0)\left[(\eta(x) - b)/(\eta_0 - b)\right]} \left\{ \frac{\eta_l - b}{\eta_l} + \frac{b}{\eta_l} \frac{1 + (n_u k_u \eta_l \, l/Q_0)\left[(\overline{\eta(x) - b})/(\eta_0 - b)\right]}{1 + n_l k_l \eta_l \, l/Q_0} \right\} \tag{41}$$

We emphasize that Equation (7) can be used to estimate η_0 only when $|N| > 0$. This approximation and that expressed in (25) for $C_u(x,t)$ are not valid when $N \to 0$. In fact, it was observed that the convergence of the integrals in (28) and (29) slows down considerably as N is chosen arbitrarily smaller. The case of negligible recharge requires a separate analysis which is currently under investigation. Equation (41) can still be applied to riparian zones whenever η_0 can be measured at the inlet boundary. In (41), k_u may account for the rate of loss by denitrification in the organic-rich stream valley sediments and uptake by the vegetative cover (e.g., trees and shrubs) in the riparian buffer.

4. Regional Ground-water Flow and Nitrate Transport and Fate Model

A regional ground-water flow model is being developed, which covers the paired watersheds and extends from north at the Sassafras River to south at the Chester River. The objective of the model is: 1) to estimate regional water levels and total ground-water discharge (base flow) to Morgan Creek and the Chesterville Branch; and 2) to estimate total nitrate base-flow discharge to the Chester River in relationship to potential deep denitrification. The model is developed using the GMS model which implements MODFLOW, MODPATH, and MT3D modules within user friendly Graphical User Interface (GUI). Because of the complexity of the hydrostratigraphy and drainage network in the Locust Grove site, the effort comprised of the following major steps: 1) development of the geologic model from core data (e.g., Figure 6(c)); 2) development of the conceptual model, including recharge distribution, imposition of boundary conditions, leakance between hydrostratigraphic layers and aquifers, and delineation of the surface-water drainage network and related hydraulic properties (Figure 14); and 3) numerical simulations and calibration. Two models are considered; a one-layer model and a four-layer model. In the latter, the surficial (Columbia/Aquia) aquifer was separated into an upper (oxic) and lower (redox) layer, and the lower Hornerstown and Monmouth aquifers were represented with two distinct layers.

Because the northern and southern boundaries of the ground-water flow domain coincide with the Sassafras River and the Chester River, respectively, a prescribed-head boundary of zero is assumed on each boundary. The western boundary (Figure 14) delineates the surface-water drainage boundary and, therefore, is assumed to approximate a ground-water divide, and a no-flow boundary thereby is imposed there. On the east side, however, two types of boundary conditions were considered: 1) a no-flow boundary along the surface-water drainage divide (to the east of Mills Branch); and 2) a prescribed-head along Mills Branch, with the head equal to the surface elevation along the Creek, and to the north of this Creek toward the Sassafras by interpolation with reported observed heads. Figures 15 and 16 show the GMS simulated heads for the wet season (November-April), which is characterized by high evapotranspiration, for the two scenarios of no-flow boundary and a prescribed-head boundary on the east side of the ground-water flow domain. The two boundary conditions produced almost similar head distribution, except that a well-defined mound is produced between Morgan Creek, Chesterville Branch, and Mills Branch, when the latter creek is used as a prescribed-head boundary (Figure 15). Figure 17 shows ground-water flow directions during the wet season for the one-layer model. It is clear that ground-water flow is eventually discharged as base flow to the surface-water drainage system.

Figures 18-21 compare simulated heads with observed seasonally-averaged water levels for the wet (November-April) and dry (May-October) seasons, and the comparisons for the different flow scenarios mentioned above were quite remarkable. Figure 22 compares the simulated surface-water discharge in the Morgan Creek to observed values at the stream gauge stations (labeled with triangles in Figure 6(a)) during both seasons. Because of relative homogeneity of the surficial aquifer, the hydraulic conductivity was assumed to be 16.76 m/d as justified in the above section. The recharge was calibrated for a high value of 0.0016 m/d and a low value of 0.0012 m/d and the calibrated recharge values for the dry season were one-tenth of the wet season recharge values. The close comparison between the estimated and observed stream discharges may verify a fairly good model performance given the complexity of the actual drainage network.

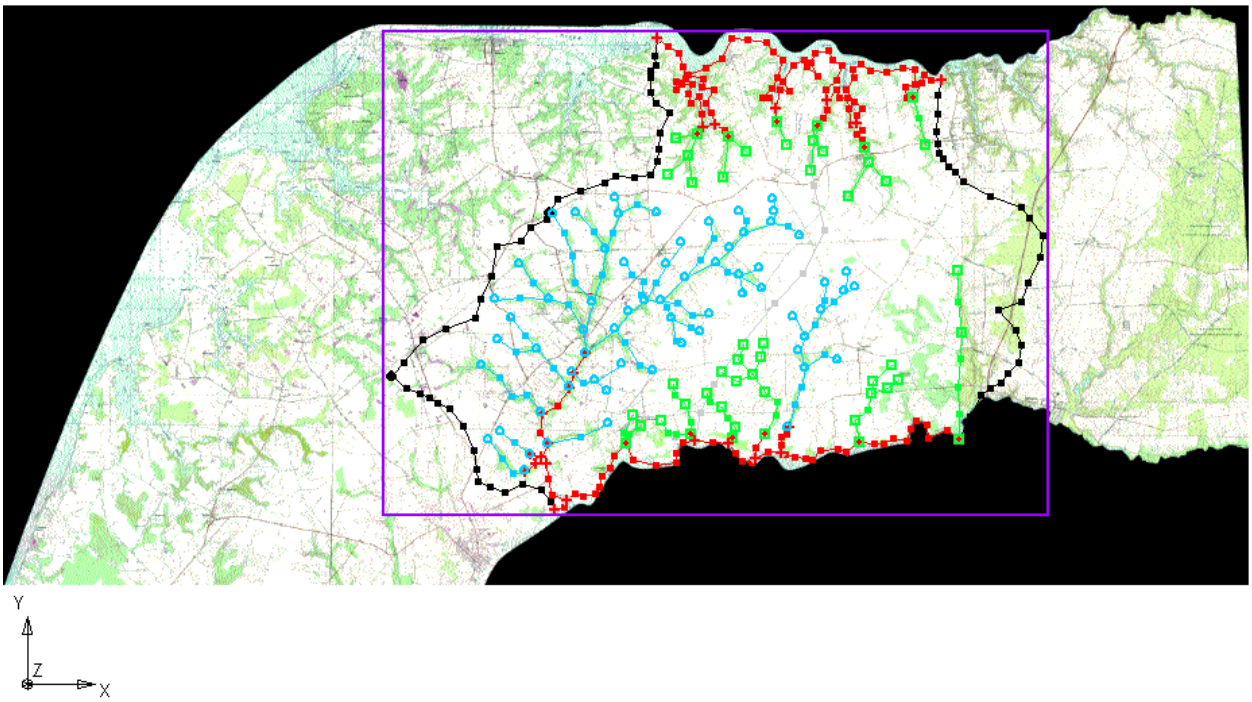

Figure 14. Regional ground-water conceptual model including surface-water drainage network, with the prescribed head equal to zero (sea level) at the Sassafras River to the north and the Chester River to the south, and no-flow boundary elsewhere.

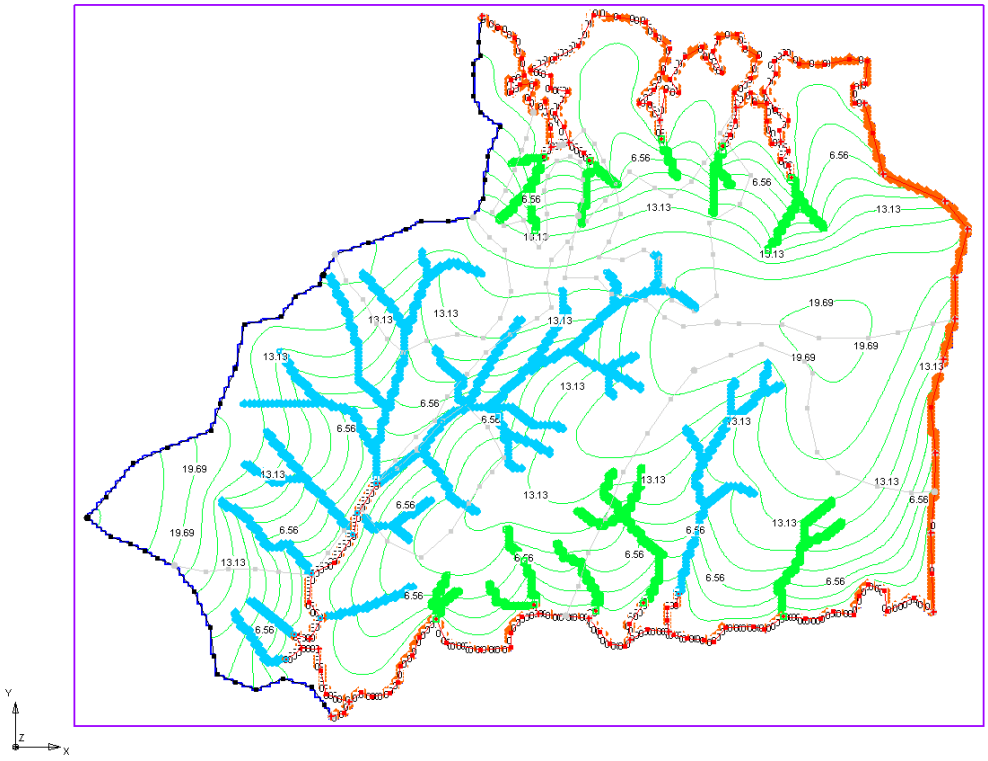

Figure 15. Simulated steady-state ground-water heads in the wet-season (Nov.-Apr.) for the case of prescribed heads along Mills Branch located on the eastern border of the flow domain.

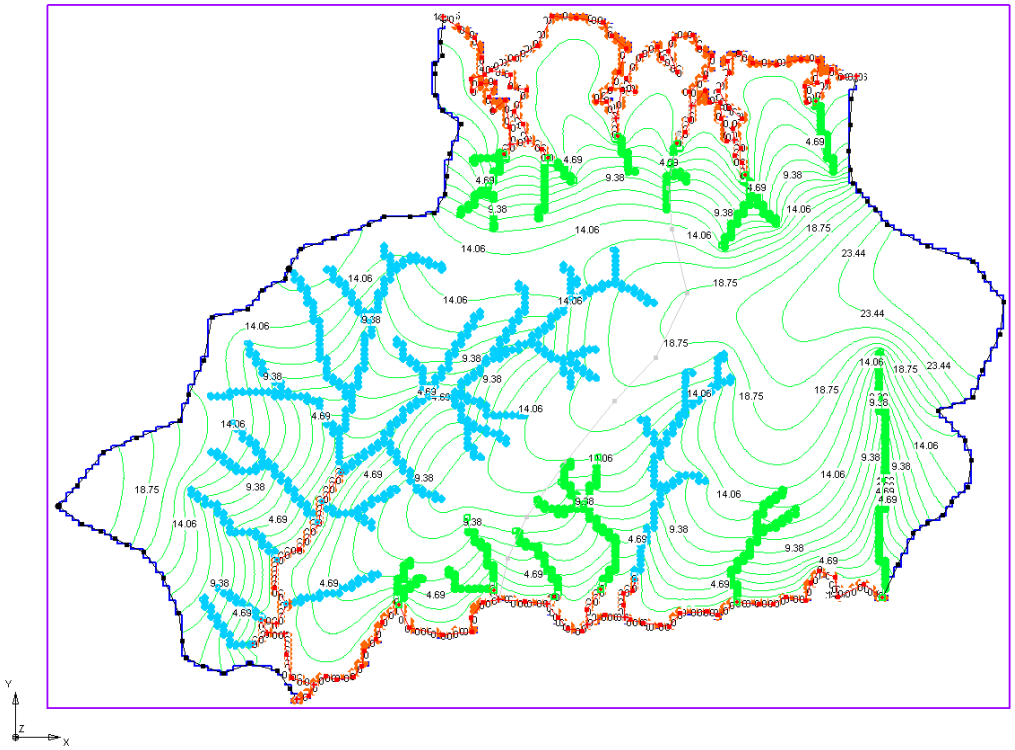

Figure 16. Simulated steady-state ground-water heads in the wet season (Nov.-Apr.) for the case of no-flow boundary on the eastern border of the flow domain.

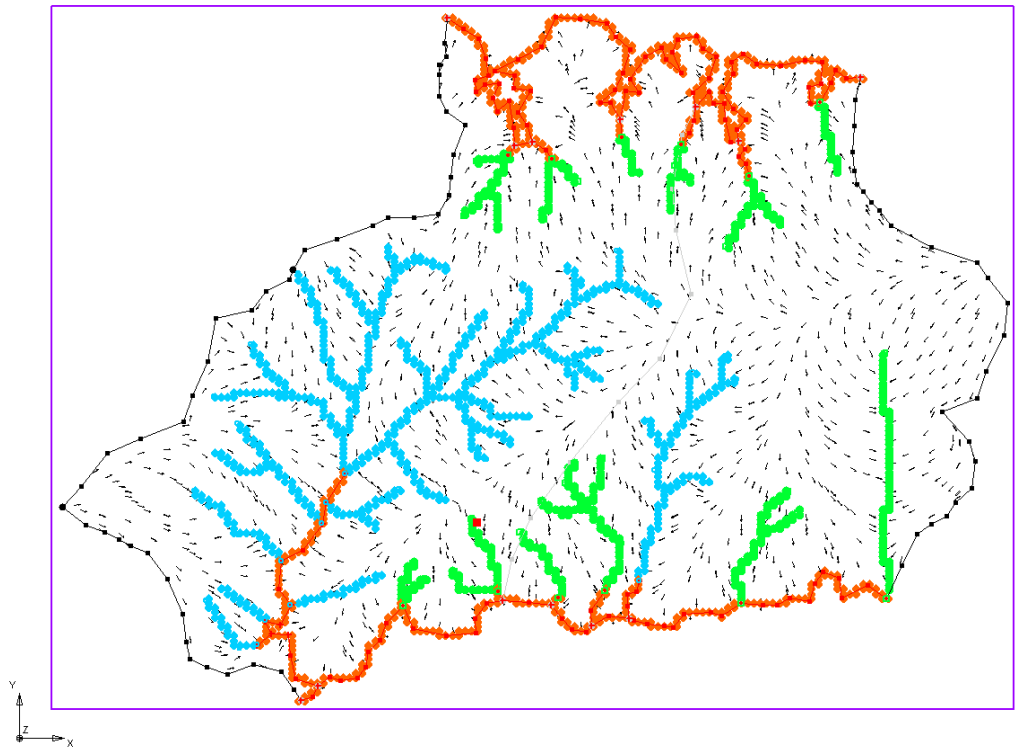

Figure 17. Ground-water flow directions simulated in the wet season (Nov.-Apr.) for a one-layer model.

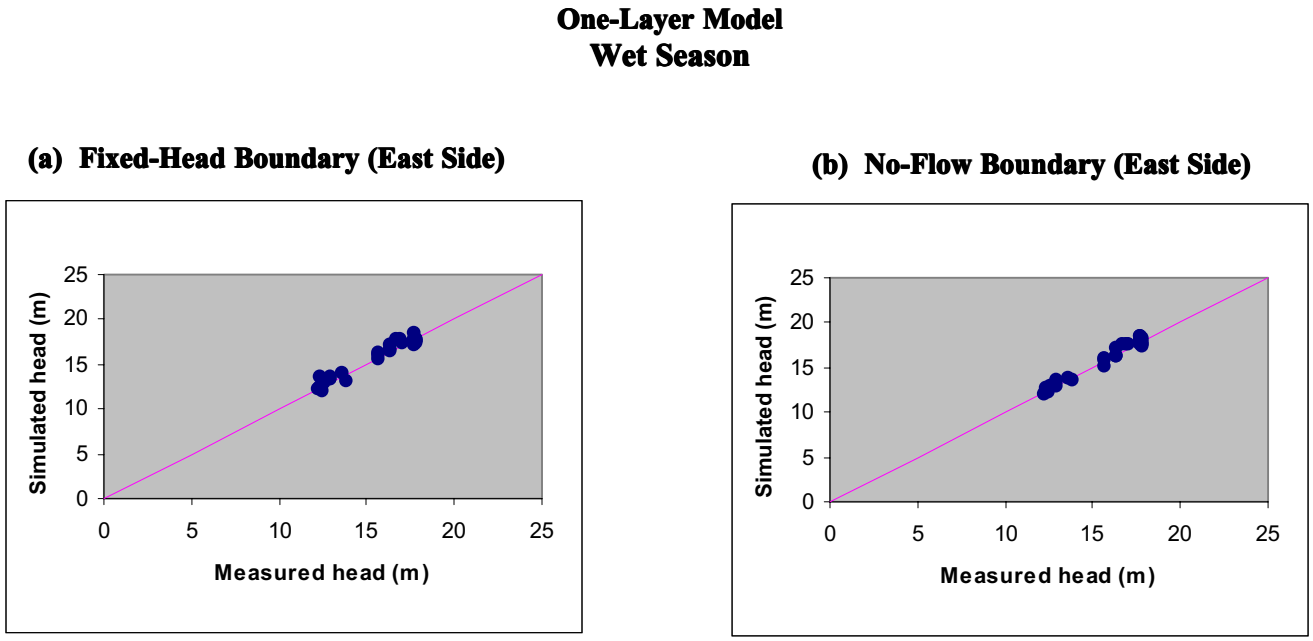

Figure 18. Simulated versus measured heads in the wet season (Nov.-Apr.) for a one-layer model: (a) prescribed-head on the east side, and (b) no-flow boundary on the east side.

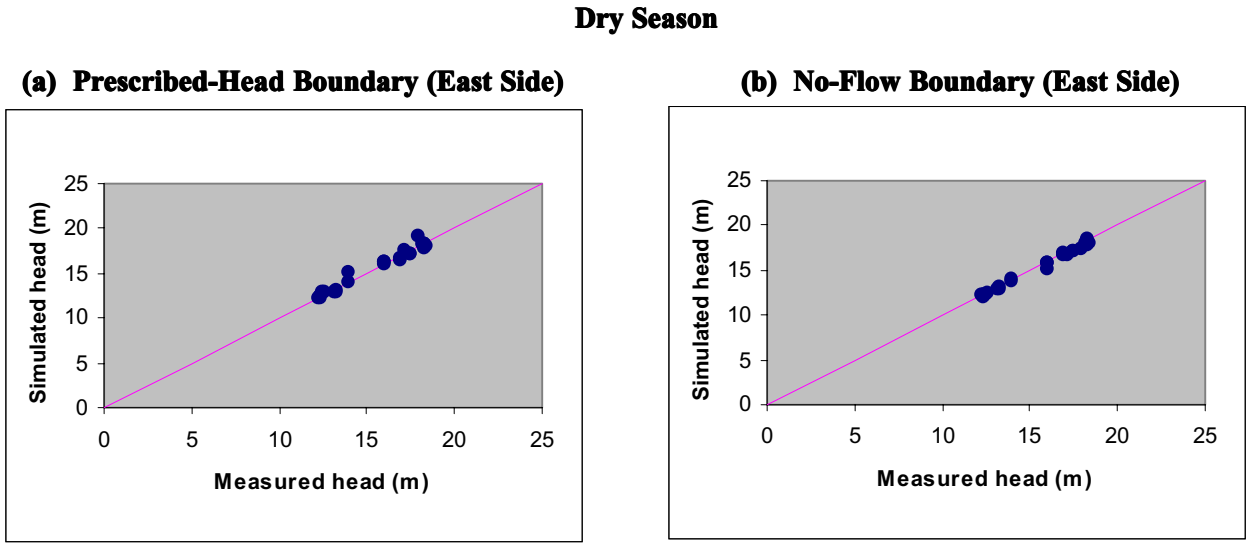

Figure 19. Simulated versus measured heads in the dry season (May-Oct.) for a one-layer model: (a) prescribed-head on the east side, and (b) no-flow boundary on the east side.

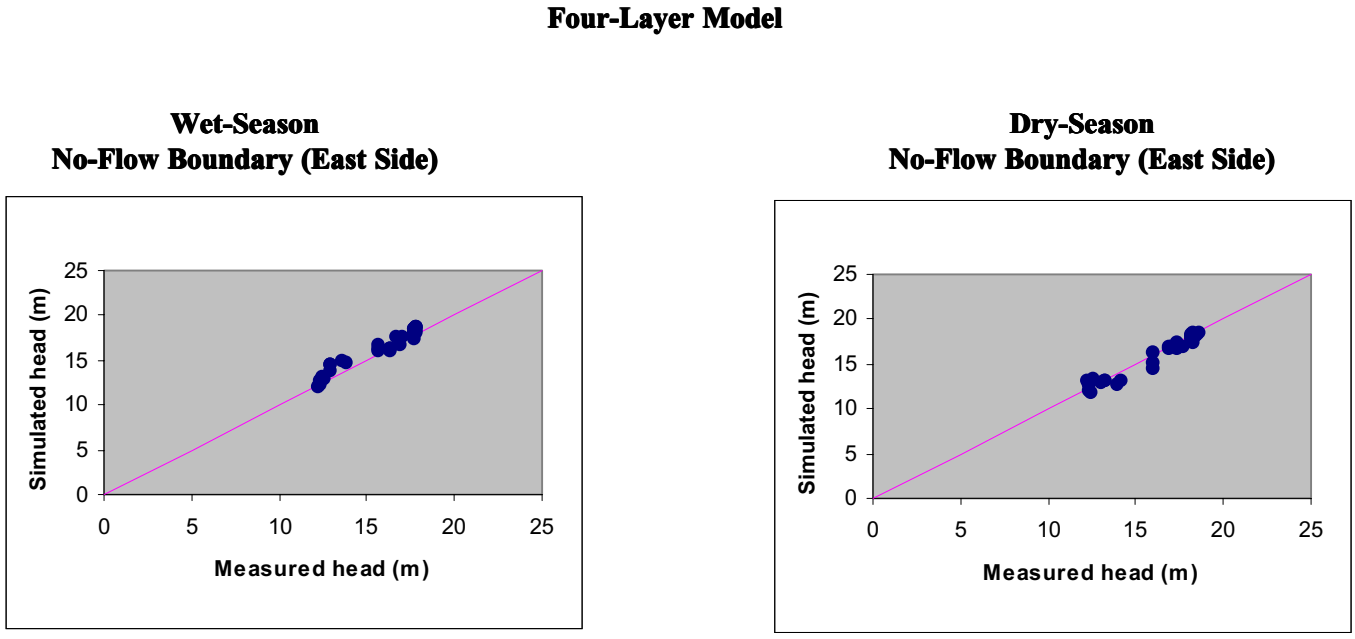

Figure 20. Simulated versus measured heads at surficial aquifer (four-layer model with no-flow boundary on the east side): (a) wet-season (Nov.-Apr.), and (b) dry season (May-Oct.).

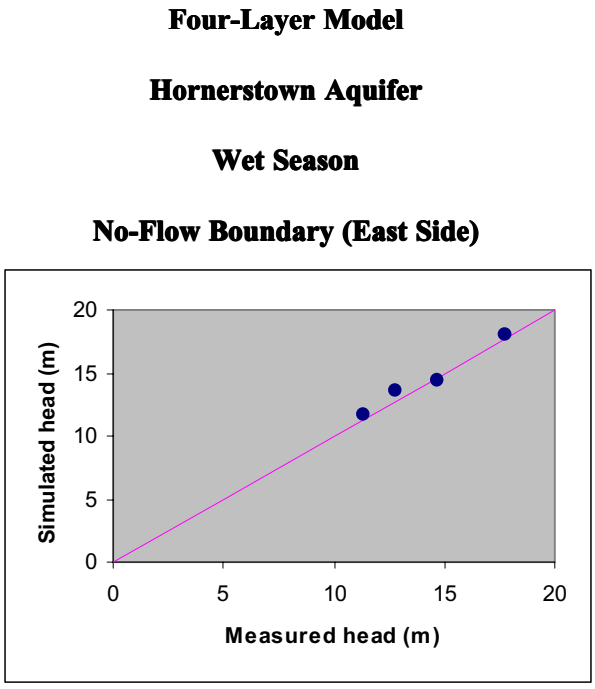

Figure 21. Simulated versus measured heads at Hornerstown aquifer in wet season (Nov.-Apr.) (four-layer model with no-flow boundary on the east side).

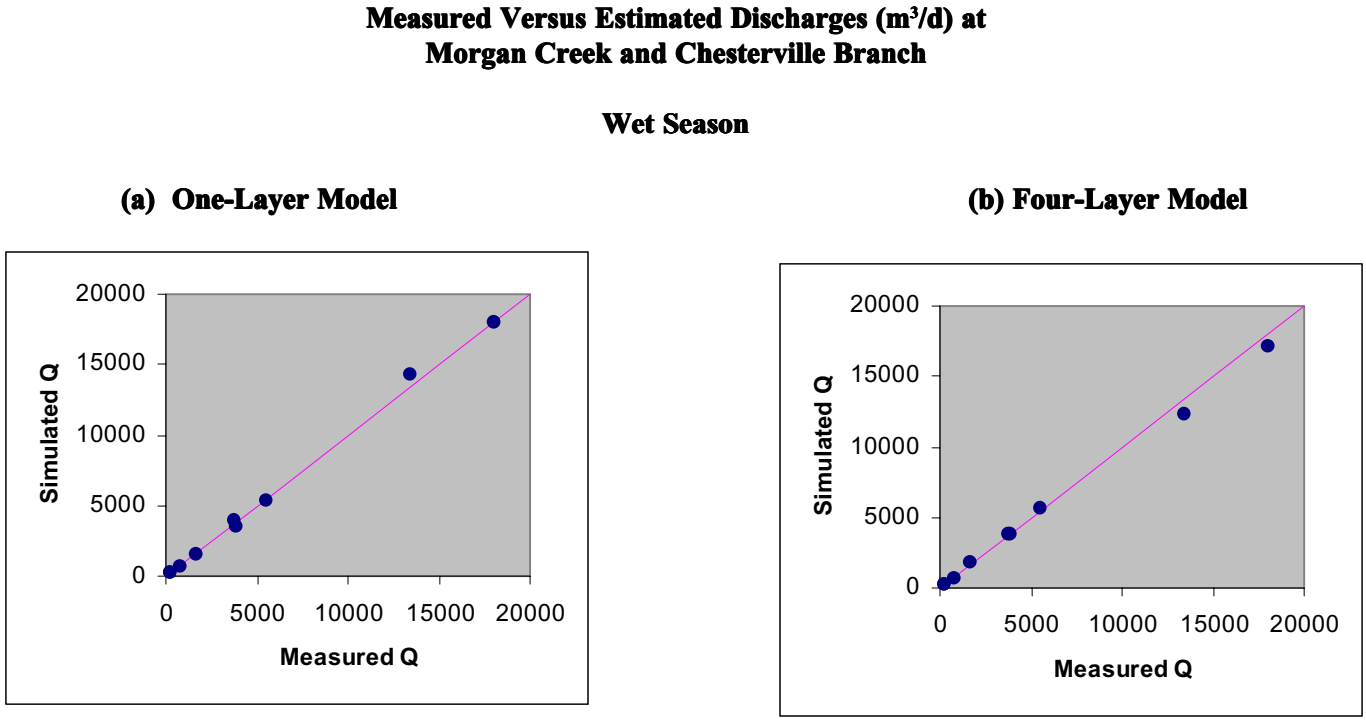

Figure 22. Simulated versus measured stream-flow discharges at Morgan Creek in the wet season (Nov.-Apr.) (no-flow boundary on the east side): (a) one-layer model, and (b) four-layer model.

The integrity of the ground-water flow model will be critical in the assessment of the nitrate fate and transport in ground water and the estimation of the capacity of the ground-watershed to reduce nitrogen loading to the Chester River by the process of deep denitrification. Refining the model is planned in the coming year, and field measured values for the hydraulic conductivity and transmissivities of the lower aquifers will be obtained using slug and pumping tests in order to improve the model performance. It is worth pointing out that it is not clear if any further calibration is worthwhile in light of the remarkably good reproduction of the observed heads and stream discharges by the numerical model.

5. Summary, Conclusions, and Future Directions

Two adjacent watersheds in the mid-Atlantic coastal plain show significant disparity in base-flow nitrate levels. It is likely that a combination of deep denitrification (reducing subsurface sediments) and historical input variation are mainly responsible for the disparity in observed base-flow nitrate levels. Until recently, previous studies focused on the effects of shallow riparian zone reactions on nitrogen reduction in the discharging ground waters, and with less emphasis on deep denitrification as an integral part of the riparian zones. In this joint effort between the USEPA and the USGS, a well network has been established at the site for survey of synoptic water levels and nitrate concentrations in ground water and at surface water discharge to the Morgan Creek and the Chesterville Branch. A scientific framework has been developed based on the laws of physics and conservation of mass in order to assess potential impact of deep denitrification on the reduction of nitrate discharge to surface waters. The framework varies from local scale to the regional scale. The former involves the development of analytical characteristic solutions, which aim at understanding the impact of geohydrologic factors, such as ground-water-flow pattern and geometric setup of hydrostratigraphy, on the potential for nitrate reduction by denitrification. Also, a simple index is developed using basic physical principles, which may be used as a measure of the removal capacity for nitrate in ground-watersheds. At a larger scale, a regional model is being developed for the area, which aims at exploring the impact of denitrification in the subsurface on the overall nitrate budget at the watershed scale.

Analysis based on the local-scale hydrologic and transport models indicated that the observed differences in base-flow nitrate levels between the two watersheds may be explained on the basis of denitrification in relatively deep subsurface reducing sediments. The models predicted a much greater capacity to reduce nitrate levels at the discharge point in

Morgan Creek as opposed to the Chesterville Branch. The regional dip of the strata resulted in a relatively shallower redox zone below Morgan Creek as opposed to the Chesterville Branch, and this, in combination with the ground-water flow pattern and historical input variations, resulted in greater denitrification in the former watershed. Although these results are consistent with the reported field findings, the observed nitrate levels in the discharging ground waters below the Chesterville Branch were remarkably lower than theoretical predictions. This indicates that other processes may be responsible for removal, such as denitrification in peat-rich stream valley sediments. The local-scale framework, however, is adaptable to integrate deep denitrification and removal at the ground-water-surface water interface as an integral element of the self-purifying nature of riparian zones. Indices were developed and proposed for the assessment of the removal capacity of watersheds for nitrate in ground water. The indices relate nitrate reduction in stream riparian zones to potential denitrification in subsurface reducing sediments and organic-rich stream-valley alluvium, and the geometric and hydraulic properties of the underlying aquifer. The implication of the findings may be twofold. First, they emphasized the possible role of deep denitrification as an integral element of riparian woodlands on nitrate reductions. Second, the models, including the removal efficiency indices, may be used as management tools for agricultural practices in agricultural watersheds where effective subsurface denitrification ocurrs. Although not conclusive, the presented analysis indicates that deep denitrification has a potential for significantly reducing nitrate loading in ground-water discharge to streams, such as the case in Morgan Creek. The analysis was based on county-level averaged net nitrate input to ground water. The impact of the spatial variablility of nitrate at the source can be significant in the interpretation of base-flow nitrate loadings, and needs to be addressed in future studies. Additional field work and analysis is needed to support this theory and to resolve the effectiveness of deep denitrification from other processes responsible for nitrate removal in riparian zones, such as denitrification in organic-rich stream valley sediments, assimilation by plants, immobilization by bacteria, or microbial nitrate ammonification. The capacity for nitrate removal by riparian buffer zones is not completely understood, including processes occurring within soils and streams. More intensive sampling would be required to confirm the effectiveness of deep denitrification on nitrate removal, including sampled synoptic base-flow nitrate levels below each creek and across the peat-rich stream valley sediments. This is planned for FY 2000 as a supplement to the current IAG project, including sampling from 33 new wells, in addition to extensions of the theoretical framework and the development of the regional nitrate transport and fate model. The network includes multilevel and multiport wells, which are bracketing the redox zone. Planned, also, is the implementation of the proposed NO^-_3 removal capacity index I_{RC} in GIS for the Locust Grove study area for the purpose of delineating watersheds according to their potential removal efficiency for ground-water nitrate, and develop maps as tools for management purposes. The research is expected to provide a scientific modeling foundation and insights into the removal of nitrate in riparian environments, with implications on nitrogen management in agricultural watersheds.

Appendix A

The integration of (1) yields

$$K\,\eta\frac{dh}{dx}+N\,x=C \tag{A1}$$

in which C is a constant that can be obtained by imposing boundary condition (3a),

$$K\,\eta\frac{d}{dx}(\eta+\beta\,x)+N\,x=-Q_0 \tag{A2}$$

After multiplying (A2) by dx and using the following linear transformation

$$\xi=N\,x+Q_0 \tag{A3}$$

Equation (A2) can be expressed as

$$\eta\,d\eta+\frac{\beta}{N}\eta\,d\xi+\frac{1}{K\,N}\xi\,d\xi=0 \tag{A4}$$

Consider the transformation

$$\eta(x)=\nu(x)\,\xi(x) \tag{A5}$$

which if used in (A4) yields the following ordinary differential equation

$$(\nu^2+\frac{\beta}{N}\nu+\frac{1}{K\,N})\,d\xi+\nu\,\xi\,d\nu=0 \tag{A6}$$

The dependent and independent variables can now be separated:

$$\frac{d\xi}{\xi}+\frac{\nu\,d\nu}{\nu^2+(\beta/N)\,\nu+1/(KN)}=0 \tag{A7}$$

After adding and subtracting the same term from the left-hand side of (A7) and completing the square in the denominator, one obtains

$$\frac{d\xi}{\xi}+\frac{1}{2}\frac{(2\nu+\beta/N)\,d\nu}{\nu^2+(\beta/N)\,\nu+1/(KN)}-\frac{\beta}{2N}\frac{d\nu}{(\nu+\beta/(2N))^2+\gamma^2}=0 \tag{A8}$$

where

$$\gamma^2=\frac{1}{KN}-\frac{1}{4}\frac{\beta^2}{N^2} \tag{A9}$$

Thus,

$$\int\frac{d\xi}{\xi}+\frac{1}{2}\int\frac{(2\nu+\beta/N)\,d\nu}{\nu^2+(\beta/N)\,\nu+1/(KN)}-\frac{\beta}{2N}\int\frac{d\nu}{(\nu+\beta/(2N))^2+\gamma^2}=0 \tag{A10}$$

The third integral can be put in a form readily available for integration if we define the new variable $u = (\nu + \beta/(2N))/\gamma$, then $du = (1/8)dz$, and

$$\int \frac{d\xi}{\xi} + \frac{1}{2}\int \frac{(2\nu + \beta/N)\,d\nu}{\nu^2 + (\beta/N)\nu + 1/(KN)} - \frac{\beta}{2N\gamma}\int \frac{du}{u^2+1} = 0 \tag{A11}$$

The evaluation of the integrals in (A11) is straightforward:

$$\ln\xi + \frac{1}{2}\ln\left|\nu^2 + \frac{\beta}{N}\nu + \frac{1}{KN}\right| - \frac{\beta}{2N\gamma}\tan^{-1} u = a_1, \qquad \text{if } \gamma \text{ is a real number} \tag{A12a}$$

$$\ln\xi + \frac{1}{2}\ln\left|\nu^2 + \frac{\beta}{N}\nu + \frac{1}{KN}\right| + \frac{\beta}{2N\sqrt{|\gamma^2|}}\coth^{-1} u = a_1, \qquad u = \frac{\nu + \frac{\beta}{2N}}{\sqrt{|\gamma^2|}} \quad \text{if } \gamma \text{ is a complex number} \tag{A12b}$$

in which a_1 is a constant of integration to be determined by imposing the boundary condition (3b). Hereafter we consider the realistic case of $\gamma^2 \geq 0$. The solution (A12b) may be used in the case of negative recharge (e.g., when evapotranspiration exceeds infiltration). The substitution for ν and u in to (A12) and taking the exponential of both sides should yield

$$\left\{\eta(x)^2 + \frac{\beta}{N}\eta(x)(N\,x + Q_0) + \frac{1}{KN}(N\,x + Q_0)^2\right\}\cdot\exp\left\{-\frac{\beta}{N\gamma}\tan^{-1}\left(\frac{\frac{\eta(x)}{N\,x + Q_0} + \frac{\beta}{2N}}{\gamma}\right)\right\} = a_2 \tag{A13}$$

in which a_2 is a constant, which can be obtained by evaluating (A13) at $x = l$ after taking the exponential of both sides and substituting η_l for $\eta(l)$, to yield

$$\eta^2 + (\beta/N)\eta(N\,x + Q_0) + (1/KN)(N\,x + Q_0)^2 = \kappa$$

$$\cdot\exp\left\{-\frac{\beta}{\gamma N}\left[\tan^{-1}\left(\frac{\eta_l/(Nl + Q_0) + \beta/(2N)}{\gamma}\right) - \tan^{-1}\left(\frac{\eta(x)/(Nx + Q_0) + \beta/(2N)}{\gamma}\right)\right]\right\} \tag{A14}$$

where

$$\kappa = \eta_l^{\,2} + (\beta/N)\eta_l(N\,l + Q_0) + (1/KN)(N\,l + Q_0)^2 \tag{A15}$$

The substitution of the asymptotic expansion (7) into (4), after expanding the right-hand side in Taylor series about $\beta = 0$, should yield

$$\phi_0{}^2 + 2\phi_0\phi_1\beta + \frac{1}{N}\phi_0(Nx+Q_0)\beta + O[\beta^2] + \frac{1}{KN}(Nx+Q_0)^2 = \eta_l{}^2 + \frac{1}{KN}(Nl+Q_0)^2$$
$$+ \frac{\eta_l}{N}\cdot(Nl+Q_0)\beta - \left(\eta_l{}^2 + \frac{1}{KN}(Nl+Q_0)^2\right)\sqrt{\frac{K}{N}}\left[\tan^{-1}\left(\sqrt{KN}\,\frac{\eta_l}{Nl+Q_0}\right)\right.$$
$$\left. - \tan^{-1}\left(\sqrt{KN}\,\frac{\phi_0(x)}{Nx+Q_0}\right)\right]\beta + O[\beta^2] \tag{A16}$$

Thus, by collecting terms of equal order in β, we have the following equations for the zero-order term, $\beta^{(0)}$:

$$\phi_0(x)^2 + \frac{1}{KN}(Nx+Q_0)^2 = \eta_l{}^2 + \frac{1}{KN}(Nl+Q_0)^2 \tag{A17}$$

and the first-order term, $\beta^{(1)}$:

$$2\phi_0\phi_1 + \frac{1}{N}\phi_0(Nx+Q_0) = \frac{\eta_l}{N}\cdot(Nl+Q_0) - \left(\eta_l{}^2 + \frac{1}{KN}(Nl+Q_0)^2\right)\sqrt{\frac{K}{N}}$$
$$\cdot\left[\tan^{-1}\left(\sqrt{KN}\,\frac{\eta_l}{Nl+Q_0}\right) - \tan^{-1}\left(\sqrt{KN}\,\frac{\phi_0(x)}{Nx+Q_0}\right)\right] \tag{A18}$$

Equation (A17) can be solved directly to yield (8), which after the substitution into (A18) and solving for $\phi_1(x)$ results in (9).

Equations (13) and (14) follow immediately by substituting the asymptotic expansion of (7) for $\eta(x)$ in (11)

$$Q_l(x) \sim (Nx+Q_0)\frac{b}{\phi_0(x)}\frac{1}{1+(\phi_1(x)/\phi_0(x))\beta+\ldots} \tag{A19}$$

and expanding the quotient in Taylor series about $\beta = 0$,

$$Q_l(x) \sim (Nx+Q_0)\frac{b}{\phi_0(x)}\left(1-\frac{\phi_1(x)}{\phi_0(x)}\beta+\ldots\right) \tag{A20}$$

The approximation (14) for $Q_u(x)$ can be obtained directly by subtracting (A20) from $Q_T(x)$ or by the substitution of (7) into (12) and following the same procedure above.

Appendix B

In this section we derive the differential equations that govern the zero- and first-order concentrations. We start by dividing Equation (18) by $Q_u(x)$

$$n\frac{\eta(x)-b}{Q_u(x)}\frac{\partial C_u}{\partial t}+\frac{\partial C_u}{\partial x}+\frac{N+n\,k_u\,(\eta(x)-b)}{Q_u(x)}C_u=\frac{N}{Q_u(x)}C^*[x,t(x))] \tag{B1}$$

and introducing the following characteristic time relationship:

$$\frac{dt}{dx}=n\frac{\eta(x)-b}{Q_u(x)} \tag{B2}$$

Since it is known from calculus that total derivative (or convective derivative) is given by

$$\frac{d\psi_0}{dx}=\frac{\partial\psi_0}{\partial x}+\frac{\partial\psi_0}{\partial t}\frac{dt}{dx} \tag{B3}$$

Then, (B1) can be written in the following Lagrangian form

$$\frac{dC_u}{dx}+\frac{N+n\,k_u\,(\eta(x)-b)}{Q_u(x)}C_u=\frac{N}{Q_u(x)}C^*[x,t(x))] \tag{B4}$$

The coefficient of C_u and C^* can be expanded in Taylor series about $\beta = 0$ after substituting (12) for $Q_u(x)$, and (7) for $\eta(x)$,

$$\begin{aligned}\frac{N+n\,k_u\,(\eta(x)-b)}{Q_u(x)} &\approx \frac{1}{N\,x+Q_0}\left\{\left(\frac{N\,\phi_0(x)}{\phi_0(x)-b}+n\,k_u\phi_0(x)\right)+\left(n\,k_u\phi_1(x)-\frac{N\,b\,\phi_1(x)}{(\phi_0(x)-b)^2}\right)\beta\right\}\\ &\approx f_1(x)+f_2(x)\beta\end{aligned} \tag{B5}$$

and

$$\begin{aligned}\frac{N}{Q_u(x)} &\approx \frac{N}{Q_0+N\,x}\left(\frac{\phi_0(x)}{\phi_0(x)-b}-\frac{b\,\phi_1(x)}{(\phi_0(x)-b)^2}\beta\right)\\ &\approx f_3(x)+f_4(x)\beta\end{aligned} \tag{B6}$$

Equation (B4) can be written after the use of (7), (12), (B5), and (B6) as

$$\frac{d\psi_0}{dx} + \frac{d\psi_1}{dx}\beta + \ldots + \left(f_1(x) + f_2(x)\beta + \ldots\right)\left(\psi_0 + \psi_1\beta + \ldots\right) = \left(f_3(x) + f_4(x)\beta + \ldots\right)C^*[x, t(x)] \tag{B7}$$

Thus, by collecting terms of equal powers in β , we have the following ordinary differential equations for the zero- and first-order approximations of ψ_u:

β^0:

$$\frac{d\psi_0}{dx} + f_1(x)\,\psi_0 = f_3(x)\,C^*[x, t(x)] \tag{B8}$$

β^1:

$$\frac{d\psi_1}{dx} + f_1(x)\,\psi_1 + f_2(x)\,\psi_0 = f_4(x)\,C^*[x, t(x)] \tag{B9}$$

Equation (B8) is equivalent to (26), and (27) follows immediately by inserting for $f_1(x)$, $f_2(x)$, and $f_3(x)$ in (B9) and arranging terms. The solutions are given in (28) and (29) by multiplying both sides of each equation by the integration factor and integrating from t_o to t and x_o to x

$$\int_{x_0}^{x} d(\psi_0(\xi)\,g(\xi)) = \int_{x_0}^{x} \frac{N}{Q_0 + N\,\xi}\,\frac{\phi_0(\xi)}{\phi_0(\xi) - b}\,C^*[\xi, t(\xi)]\,g(\xi)\,d\xi \tag{B10}$$

and

$$\int_{x_0}^{x} d(\psi_1(\xi)\,g(\xi)) = \int_{x_0}^{x} \left(f_4(\xi)\,C^*[\xi, t(\xi)] - f_2(\xi)\,\psi_0(\xi)\right)g(\xi)\,d\xi \tag{B11}$$

where

$$g(x) = \exp\left\{\int \frac{1}{Q_0 + N\,x}\left(\frac{N\,\phi_0(x)}{\phi_0(x) - b} + n\,k_u\phi_0(x)\right)dx\right\} \tag{B12}$$

The integral on the right-hand side is carried on in Appendix (C) as given by Equation (30).

A zero-order n approximation to Equation (21) can be obtained by substituting (10) and (12) for $Q_u(x)$,

$$\frac{dt}{dx} = n\,\frac{\eta(x)}{Q_0 + N\,x} \tag{B13}$$

Thus,

$$\frac{dt}{dx} \approx n\,\frac{\phi_0(x)}{Q_0 + Nx} + n\beta\,\frac{\phi_1(x)}{Q_0 + Nx} \tag{B14}$$

The integration of the zero-order term from t_o to t and x_o to x yields:

$$t - t_0 \approx n\int_{x_0}^{x} \frac{\phi_0(u)}{Q_0 + N\,u}\,du \tag{B15}$$

This integral is evaluated in Appendix C to yield

$$t(x) \approx t_0 + \frac{n}{N}\left(\phi_0(x) - \phi_0(x_0)\right) - \frac{n}{2N}\sqrt{a^*}\left\{\ln\left(\frac{\sqrt{a^*} + \phi_0(x)}{\sqrt{a^*} - \phi_0(x)}\right) - \ln\left(\frac{\sqrt{a^*} + \phi_0(x_0)}{\sqrt{a^*} - \phi_0(x_0)}\right)\right\} \tag{B16}$$

in which a^* is given by (31).

Appendix C

1- $I_1 = \int \frac{\phi_0(x)}{Q_0 + N\,x} dx$

Consider the transformation

$$\frac{1}{K\,N}(N\,x + Q_0)^2 = a^* \cos^2 u \tag{C1}$$

Taking the derivatives of both sides yields

$$\frac{2}{K}(N\,x + Q_0)\,dx = -2\,a^* \cos u\ \sin u\,du \tag{C2}$$

By substituting for $\phi_0(x)$ and using the transformations (C1) and (C2), the above integral can be written as

$$I_1 = -\frac{\sqrt{a^*}}{N}\int \frac{\sin^2 u}{\cos u} du \tag{C3}$$

The use of the fundamental trigonometric identity $\sin^2 u + \cos^2 u = 1$ in (C3) yields

$$I_1 = -\frac{\sqrt{a^*}}{N}\left\{\int \frac{1}{\cos u} du - \int \cos u\,du\right\} \tag{C4}$$

From *Gradshteyn and Ryzhik* (1994), we have

$$\int \frac{1}{\cos u} du = \ln\sqrt{\frac{1+\sin u}{1-\sin u}} + c \tag{C5}$$

in which c is an arbitrary constant. Thus,

$$I_1 = -\frac{\sqrt{a^*}}{N}\left\{\ln\sqrt{\frac{1+\sin u}{1-\sin u}} - \sin u\right\} + c \tag{C6}$$

Using (C1) and the above trigonometric identity, it can be shown that

$$\sin u = \frac{1}{\sqrt{a^*}}\phi_0(x) \tag{C7}$$

The use of (C7) in (C6) yields

$$I_1 = -\frac{\sqrt{a^*}}{2N}\ln\frac{\sqrt{a^*} + \phi_0(x)}{\sqrt{a^*} - \phi_0(x)} + \frac{1}{N}\phi_0(x) + c \tag{C8}$$

2- $$I_2 = \int \left\{\frac{N}{Q_0 + N\,x}\left(\frac{\phi_0(x)}{\phi_0(x) - b}\right) + n\,k_u \frac{\phi_0(x)}{Q_0 + N\,x}\right\} dx$$

We seek the first integral since the second is evaluated above and is given by n k_u I_1:

$$I_3 = \int \frac{N}{Q_0 + N\,x}\left(\frac{\phi_0(x)}{\phi_0(x) - b}\right)dx \tag{C9}$$

First, we express (C9) as the sum of two integrals,

$$I_3 = \int \frac{N}{Q_0 + N\,x}dx + \int \frac{N\,b}{(Q_0 + N\,x)(\phi_0(x) - b)}dx \tag{C10}$$

The evaluation of the first integral in (C10) is straightforward,

$$\int \frac{N}{Q_0 + N\,x}dx = \ln(Q_0 + N\,x) + c \tag{C11}$$

In the second integral (referred to I_4) in (C10), we introduce the transformation

$$u^2 = a^* - \frac{1}{K\,N}(Q_0 + N\,x)^2 \tag{C12}$$

Taking the derivative of both sides yields

$$2\,u\,du = -\frac{2}{K\,N}(Q_0 + N\,x)N\,dx \tag{C13}$$

The use of (C12) and (C13) in the second integral in (C10) should yield

$$I_4 = -b\int \frac{u}{(a^* - u^2)(u - b)}du \tag{C14}$$

which can be written as

$$I_4 = -b\left\{\frac{1}{2\left(\sqrt{a^*} - b\right)}\int \frac{du}{\sqrt{a^*} - u} + \frac{1}{2\left(\sqrt{a^*} + b\right)}\int \frac{du}{\sqrt{a^*} + u} + \frac{b}{a^* - b^2}\int \frac{du}{u - b}\right\} \tag{C15}$$

in which we expressed (C14) in terms of sum of fractions,

$$\frac{u}{(a^* - u^2)(u - b)} = \frac{A_1}{\sqrt{a^*} - u} + \frac{A_2}{\sqrt{a^*} + u} + \frac{A_3}{u - b} \tag{C16}$$

and the constants A_1, A_2, and A_3, are easily obtained. Thus,

$$I_4 = \frac{b}{2\left(\sqrt{a^*} - b\right)}\ln\left(\sqrt{a^*} - u\right) - \frac{b}{2\left(\sqrt{a^*} + b\right)}\ln\left(\sqrt{a^*} + u\right) - \frac{b^2}{a^* - b^2}\ln(u - b) + c \tag{C17}$$

or

$$I_4 = \frac{b}{2\left(\sqrt{a^*} - b\right)} \ln\left(\sqrt{a^*} - \phi_0(x)\right) - \frac{b}{2\left(\sqrt{a^*} + b\right)} \ln\left(\sqrt{a^*} + \phi_0(x)\right) - \frac{b^2}{a^* - b^2} \ln\left(\phi_0(x) - b\right) + c \tag{C18}$$

Finally, since

$$I_2 = \ln(Q_0 + N\,x) + I_4 + n\,k_u\,I_1 + c \tag{C19}$$

Then Equation (30) can be easily verified by substituting (C8) for I_1 and (C17) for I_4 and taking the exponent of both sides.

Appendix D

The average thickness of ground water flow in the upper layer is given by:

$$\overline{\eta(x)-b}=\frac{1}{l}\int_0^l[\eta(x)-b]\,dx=\overline{\eta(x)}-b \tag{D1}$$

An exact expression for $\overline{\eta(x)}$ can be obtained by, first, expressing Eq. (A2) as

$$\eta\frac{d\eta}{dx}+\beta\,\eta+\frac{N}{K}x=-\frac{Q_0}{K} \tag{D2}$$

or equivalently,

$$\frac{1}{2}\frac{d\eta^2}{dx}+\beta\,\eta=-\frac{1}{K}(Q_0+N)x \tag{D3}$$

and when integrated from $x = 0$ to $x = l$ yields

$$\frac{1}{2}\left(\eta_l{}^2-\eta_0{}^2\right)+\beta\int_0^l\eta(x)\,dx=-\frac{1}{K}\left(N\frac{l^2}{2}+Q_0\,l\right) \tag{D4}$$

Thus,

$$\int_0^l\eta(x)\,dx=-\frac{1}{\beta}\left\{\frac{\eta_l{}^2-\eta_0{}^2}{2}+\frac{1}{K}\left(N\frac{l^2}{2}+Q_0\,l\right)\right\} \tag{D5}$$

Finally, the substitution of (D5) into (D1) yields the desired result in Eq. (37).

Appendix E

Pensauken Formation

The surficial Pensauken Formation consists mainly of orange and reddish brown gravelly sand composed of quartz and feldspar (*Hansen*, 1992; *Drummond*, 1998,). It forms an erosional contact with underlying units, and paleochannel fill may occur. Approximate thickness has been reported to be up to 145 feet (44 meters) (*Drummond*, 1998). It is stratigraphically equivalent to the Wicomico Formation of *Overbeck and Slaughter* (1958).

Aquia Formation

The marine Aquia Formation is a calcareous, glauconitic quartz sand that coarsens upward (*Hansen*, 1992; *Drummond*, 1998); color is olive-brown to greyish-olive with a salt and pepper aspect. *Böhlke and Denver* (1995) noted that between the noncalcareous, oxidized upper portion of the formation and the underlying calcareous glauconite sands is an approximately 2 to 3 meters thick unit (referred to earlier as the redox zone) having a relatively higher gamma signature peak corresponding to material with large amounts of interstitial clay (Figure 2). *Krantz* (personal communication, 1999) has designated this as above the Aquia Confining Layer, which shows a tight gamma signal indicating an impermeable layer underlying the redox zone.

Hornerstown Formation

The Hornerstown is a massive, fine to medium grained glauconitic sand, locally coarse. The unit is olive brown in color in its upper section and greyish olive at lower levels, maintaining a salt and pepper aspect throughout (*Hansen*, 1992). Glauconite is generally dark green, polylobate with minor alteration to limonite. A gamma ray log deflection in the upper part of the Hornerstown near its contact with the Aquia is observed (*Hansen*, 1992; *Böhlke and Denver* 1995, *Krantz*, personal communication 1998). It was likewise noted that another gamma log deflection was found near the base of the Hornerstown, reflecting higher glauconite fractions, possibly with phosphate.

Severn Formation (upper portion of Monmouth Group)

This formation is one of two formations comprising the Monmouth Group. The Severn is a much finer grained unit compared to the overlying Hornerstown Formation, consisting of dark grey, glauconitic, clayey, very fine to fine sands. It is massive with common shell fragments and a mottled texture. The Severn has a gamma ray peak near its base [according to *Hansen* (1992) it may reflect the occurrence of phosphate or a high percentage of glauconite - 65%]. Glauconite grains are dark green and relatively unaltered. The formation's basal portion, consisting of quartz grains, phosphate pebbles and shell fragments, has a sharp contact with the underlying Mt. Laurel Formation (part of the Monmouth Group).

Mt. Laurel Formation (lower part of Monmouth Group)

The Mt. Laurel Formation is the lower member of the Monmouth Group. Its lower 22 feet (6.7 meters) is composed of medium grey, clayey glauconitic (up to 35%) very fine to fine sands. Sands are calcareous with localized pelycepod concentrations and irregular calcite cemented zones. Its upper 56 feet (17 meters) is light olive grey, medium to fine silty quartzose sand. Coarser beds are less glauconitic (15%). The formation ranges in thickness from 25-80 feet (7.6-24.4 meters) in Kent County.

Matawan Group

The Matawan Group consists of a sequence of glauconitic, dark grey to olive grey silty clays and very fine to fine sands. Bedding is massive, with some mottling and suggestion of bioturbation in the form of burrows. Beds are generally noncalcareous below 320 feet in this core hole.

Appendix F

Locust Grove Database

The data reported in Tables 1 and 2 are part of a comprehensive hydrogeological database that are collected by the US Geological Survey under IAG #DW14937941. The comprehensive database will be detailed in a final report to be prepared by the USGS under this agreement, including methods, procedures, quality assurance measures, and geochemical analysis. The data will be managed by the National Risk Management Research Laboratory, U.S. Environmental Protection Agency, in Ada, Oklahoma, and will be made available on Compact Disks (CDs) for distribution, upon the completion of the project.

Quality of Data

The data in Table 1 and Table 2 show information on newly installed wells (wells KE Bf 74, 254, and 180, KE Be 171 are old), and synoptic measurements of water-table levels at the site (10/97-4/99). The objective of the data, including core samples and head measurements is to: 1) develop the stratigraphic framework of the surficial (Columbia\Aquia) unconfined aquifer, the uppermost confining layer, and the uppermost confined aquifer; 2) delineate the head distribution and flow patterns; and 3) delineate the redox zone on top of the uppermost confining layer and assess the geochemical processes controlling nitrogen concentration in the unconfined aquifer and in ground-water discharge to the streams; and 4) estimate nitrogen loads to the streams from ground-water discharge.

All new wells were installed following the protocols and procedures for well installation recommended for the USGS NAQWA program. Sampling procedures, including drilling operations, installation of wells, and measurement for heads are documented in detail in the project Quality Assurance Plan. The data from new coreholes and existing well log information were used to develop the stratigraphic framework by extrapolation over the entire study area, using the GMS Model. Figure 7(c) is an illustration to the extrapolation procedure.

Table 1. Core Data Submissions by USGS (as of July 1999; file sent 12/2/98)

USGS/MGS Well Number	Utm-x	Utm-y	Layer information available *
KE Be 185 (new)	418091.9	4353369.7	Pen, AQ, ACL, TACL, Ho, HS
KE Be 183 (new)	416392.7	4351229.6	Pen, AQ, ACL, TACL, Ho
KE Be 184 (new)	416770.7	4350732.2	Pen, AQ, ACL, TACL, Ho
KE Be 186 (new)	419691.2	4350547.5	Pen, AQ, ACL, TACL, Ho, HS
KE Bf 180	421132.6	4348590.4	Pen, AQ, ACL, TACL, Ho, HS and more (see Hansen 1992)
KE Be 171	420790.0	4347884.8	
KE Be 210 (new)	419129.7	4351848.2	
KE Be 187 (new)	415665.0	4352594.0	
KE Be 188 (new)	415901.1	4352283.1	
KE Be 189 (new)	416605.0	4350919.0	
KE Be 190 (new)	416700.1	4350856.3	
KE Be 195 (new)	417830.0	4348963.6	
KE Be 196 (new)	417893.7	4348192.2	
KE Be 197 (new)	416865.9	4352920.2	
Nau Farm (new)	416959.0	4352672.6	Pen, AQ, ACL, TACL, Ho, HS, HCL
Locust Grove corehole (new)			
KE Be 201 (new)	418106.8	4350224.8	
KE Be 202 (new)	418907.5	4351203	
KE Be 203 (new)	419002.6	4348828.1	
KE Be 204 (new)	419154.9	4349658.9	
KE-88-0146 (new)	419559.6	4349408.1	
KE Bf 74			
KE Bf 154			

* *Pen: Pensauken, AQ: Aquia, ACL: Aquia Confining Layer, TACL: ATight@ gamma peak Aquia Confining Layer, Ho: Hornerstown, HS: Hornerstown sand (?), HCL: Hornerstown Confining Layer*

Table 2. Recent Synoptic Water Table Measurements by the USGS in Locust Grove, MD

Well label	10/97	3/98	5/98	6/98	7/98	9/98	10/98	11/98	12/98	1/99	3/99	4/99
KE Bf 154		9.75	9.83	9.72	6.48	9.2	2.04	8.89	8.72	8.97	9.01	9.2
KE Bf 155		9.94	10	9.58	6.61	9.38	3.38	9.06	8.9	9.15	9.18	9.38
KE-88-0696		14.23	14.41	14.23	13.98	13.74	13.52	13.42	13.38	13.4	13.51	13.7
KE Be 216			14.4	14.23	13.97	13.74	13.52	13.41	13.38	13.4	13.51	13.7
KE Bf 186			16.11	15.84	13.3	14.83	14.78	14.2	14.65	14.75	14.88	15.12
Block 3-54		15.66	15.75	15.48	12.31	14.48	14.44	13.74	14.29	14.4	14.52	14.76
KE Bf 184			17.62	17.49	17.19	16.9	16.48	16.34	16.36	16.32	16.36	16.46
KE Bf 185			17.62	17.49	17.19	16.9	16.47	16.36	16.35	16.33	16.37	16.47
KE Be 154		17.25	17.76	17.47	15.09	17.04	15.7	16.78	16.7	16.58	16.45	16.45
KE Be 213			17.76	17.43	16.56	17.02	15.41	16.78	16.71	16.62	16.46	16.45
KE Be 214			18.26	18.19	18	17.75	17.36	17.13	17.05	16.95	16.94	17.02
KE Be 215			18.26	18.19	17.99	17.75	17.35	17.12	17.05	16.95	16.94	17.02
Block 6-12		15.78	15.95	15.8	15.49	15.27	14.95	14.67	14.74	14.8	14.92	15.07
KE-88-0695		13.1	12.97	12.92	11.63	12.67	12.23	12.67	12.71	12.79	12.79	12.86
KE Be 212			13.2	12.88	12.53	12.24	12.04	11.97	11.65	12.02	12.12	12.35
KE Be 211			13.44	13.44	13.13	13.05	12.95	12.89	12.87	12.91	12.95	13.1
KE Be 159	12.26	12.52	12.4	12.33	12.31	12.32	12.3	12.31	12.25	12.27	12.31	12.27
KE Be 160	12.26	12.5	12.44	12.38	12.29	12.32	12.22	12.24	12.24	12.24	12.28	12.3
KE Be 161	12.21	12.41	12.37	12.32	12.24	12.41	12.18	12.19	12.19	12.22	12.24	12.23
KE Be 63	12.41	12.68	12.55	12.5	12.41	12.45	12.35	12.35	12.25	12.43	12.43	12.42
KE Be 64	12.41	12.69	12.65	12.64	12.53	12.53	12.46	12.47	12.46	12.5	12.5	12.49
KE-94-0144		15.27	15.37	15.21	15.02	14.79	10.64	14.51	13.97	14.44	14.45	12.32
KE-94-0145		15.2	15.3	15.14	14.94	14.75	10.78	14.45	13.94	14.42	14.41	11.35
KE-94-0146		15.11	15.28	15.28	14.98	14.78	17.72	14.49	13.7	14.46	14.4	
KE Be 205			15.31	15.14	14.95	14.67	14.2	14.46	13.71	14.4	14.4	14.27
KE Be 203			14.44	14.28	13.74	13.84	13.69	13.63	13.53	13.47	13.45	13.51
KE Be 204			16.75	16.66	16.46	16.2	15.84	15.74	15.56	15.45	15.35	15.41
KE Be 62	15.71	16.39	16.42	16.25	16.01	15.85	15.62	15.48	15.46	15.52	15.51	15.63
KE Be 162	15.7	16.38	16.43	16.25	16	15.85	15.63	15.48	15.46	15.52	15.52	15.63
KE Be 163	15.72	16.4	16.44	16.26	16.01	15.85	15.63	15.49	15.47	15.52	15.52	15.63
KE Be 61	16.81	17.63	18.03	17.84	17.66	17.42	17	16.8	16.72	16.6	16.66	16.77
KE Be 53	16.76	17.71	18.12	17.94	17.75	17.5	17.11	16.89	16.81	16.72	16.74	16.87
KE Be 52	17.29	17.71	18.12	17.93	17.74	17.5	17.1	16.88	16.81	16.73	16.74	16.86
KE Be 59	18.06	18.81	18.76	18.78	18.5	18.26	17.94	17.74	17.63	17.62	17.58	17.76
KE Be 164	18.05	18.73	18.69	18.7	18.39	18.19	17.85	17.66	17.56	17.53	17.51	17.67
KE Be 165	17.98	18.75	18.56	18.6	18.28	18.17	17.85	17.7	17.6	17.66	17.56	17.58
KE Be 166	17.99	18.76	18.57	18.61	18.3	18.16	17.85	17.7	17.6	17.7	17.58	17.73
KE Be 167	18	18.81	18.57	18.62	18.3	18.17	17.86	17.7	17.6	17.69	17.58	17.71
KE Be 51	17.64	17.73	18.11	18.09	17.94	17.73	17.36	17.14	17.01	16.86	16.69	16.78
KE Be 207			18.54	18.58	18.24	18.07	17.87	17.74	17.61	17.61	17.56	17.8
KE Be 208			18.53	18.57	18.23	18.07	17.81	17.66	17.59	17.62	17.56	17.79
KE Be 50	17.83	19.15	18.47	18.5	18.17	17.99	17.73	17.59	17.52	17.51	17.48	17.74
KE Be 210			18.49	18.59	18.24	18.06	17.89	17.76	17.58	17.61	17.58	17.77

Table 2. Continued.

KE Be 206			18.57	18.6	18.26	18.08	17.81	17.66	17.59	17.6	17.59	17.8
KE Be 198			17.65	17.68	17.57	17.43	17.18	16.98	16.85	16.73	16.46	16.48
KE Be 199			17.65	17.69	17.58	17.44	17.2	17.16	16.86	16.83	16.7	16.72
KE Be 200			17.65	17.69	17.59	17.75	16.58	17.05	16.88	16.71	16.48	16.49
KE Be 197			17.93	17.89	17.76	17.55	17.17					
KE Be 187			19.4	20.3	19.79	20.49	19.23	19.82	19.76	20.49	20.54	20.16
KE Be 188			18.5	18.62	18.28	18.21	17.76	17.58	17.4	17.52	17.22	17.24
KE Be 189			11.67	11.64	11.53	11.54	11.62	11.48	11.46	11.45	11.43	11.54
KE Be 156		11.39	11.33	11.28	11.2	11.25	11.2	11.21	11.15	11.17	11.16	11.18
KE Be 157	12.01	12.16	12.2	12.12	12.03	12	11.89	11.86	11.86	11.88	11.82	11.88
KE Be 158		13.33	13.57	13.45	13.37	13.26	13.09	13.02	12.95	12.92	12.93	12.94
KE Be 191			13.52	13.4	13.31	13.21	13.04	12.96	12.91	12.86	12.84	12.9
KE Be 192			13.52	13.41	13.31	13.08	13.05	12.97	12.91	12.87	12.85	12.9
KE Be 193			13.53	13.42	13.33	13.23	13.06	12.99	12.92	12.88	12.86	12.92
KE Be 201			16.52	16.48	16.3	16	15.7	15.49	15.31	15.21	15.06	15.24
KE Be 60	18.05	18.05	18.58	18.44	18.33	18.4	17.69	17.48	17.55	17.15	17.02	17.15
KE Be 202			17.24	17.25	16.94	16.77	16.51	16.33	16.19	16.17	16.16	16.28
KE Be 195			17.29	17.19	17.1	16.92	16.67	16.53	16.42	16.25	16.14	16.06
KE Be 194			17.29	17.2	17.1	16.92	16.68	16.53	16.42	16.27	16.11	16.06
KE Be 196			15.58	15.52	15.43	15.32	15.11	14.97	14.87	14.74	14.6	14.54
KE Be 169												
KE Be 170												
KE Be 171												

References

Alexander, R. B., and R. A. Smith, 1990. "County-level estimates of nitrogen and phosphorus use in the United States." *U.S. Geol. Surv. Open File Rep.*, 90-130, 12 pp.

Bachman, L. J., 1984. Part 1: Hydrogeology, *in* Bachman, L.J. and J.M. Wilson, The Columbia aquifer of the Eastern Shore of Maryland: *Maryland Geological Survey Report of Investigations No. 40*, p. 1-34.

Bachman, L. J., and P. J. Phillips, 1996. Hydrologic landscapes on the Delmarva Peninsula, part 2: Estimates of base-flow nitrogen load to Chesapeake Bay. *Water Resources Bulletin*, 32(4), 779-791.

Bear J., 1972. *Dynamics of Fluids in Porous Media.* American Elsevier, New York.

Böhlke, J.K. and J.M. Denver, 1995. "Combined use of groundwater dating, chemical, and isotopic analyses to resolve the history and fate of nitrate contamination in two agricultural watersheds, Atlantic Coastal Plain, Maryland." *Water Resour. Res.*, 31, pp. 2319-2339.

Clark, W.B., 1915. Map of Kent County showing the geological formations: Maryland Geological Survey, scale 1:62,500.

Cooper, A. B., 1990. "Nitrate depletion in the riparian zone and stream channel of a small headwater catchment." *Hydrobiologia*, 202, 13-26.

Cronin. T., S. Colman, D. Willard, R. Kerhin, C. Holmes, A. Karlsen, S. Ishman, and J. Bratton, 1999. "Interdisciplinary Environmental Project Probes Chesapeake Bay Down the Core." *EOS*, 80(21).

Donigian Jr., A. S., L. C. Linker, D. Y. Alegre, C-H Chang, and R. Carsel, 1991. "Watershed Model Application to Calculate Bay Nutrient Loadings: Final Findings and Recommendations." Review Draft, Chesapeake Bay Program.

Drummond, D.D., 1998. Hydrogeology, simulation of ground-water flow, and ground-water quality of the Upper Coastal Plain aquifers in Kent County, Maryland: Maryland Geological Survey Report of Investigations No. 68, 76 p.

Gradshteyn, I. S. and I.M. Ryzhik. 1994. *Tables of Integrals, Series, and Products.* Academic Press, Inc. San Diego, CA.

Hansen, H.J., 1992. Stratigraphy of Upper Cretaceous and Tertiary sediments in a core-hole drilled near Chesterville, Kent County, Maryland: Maryland Geological Survey Open-file Report No. 93-02-7, 38 p.

Jacobs, T. C., and J. W. Gilliam. 1985. "Riparian losses of nitrate from agricultural drainage waters." *J. Environ. Qual.* 14(4), 472-478.

Kinzelbach, W., W. Schafer, and J. Herzer. 1991. "Numerical modeling of natural and enhanced denitrification processes in aquifers." *Water Resour. Res.* 27(6), 1123-1135.

Korom, S. F., 1992. "Natural Denitrification in the Saturated Zone: A Review*." Water Resour. Res.* 28(6), 1657-1668.

Krantz, D., 1998. Affiliation, Personal Communication.

Lowrance, R., R. Todd, J. Fail, Jr., O. Hendrickson, Jr., R. Leonard, and L. Asmussen, 1984. "Riparian forests as nutrient filters in agricultural watersheds." *BioScience*, 34(6), 374-377.

Meisler, H., 1986. "Northern Atlantic coastal plain regional aquifer-system study, in regional aquifer-system analysis program of the U.S. Geological Survey," Summary of projects 1978-1984, edited by R. J. Sun, *U.S. Geol. Surv. Circ.*, 1002, 168-194.

Mengis, M., S.L. Schiff, M. Harris, M. C. English, R. Aravena, R. J. Elgood, and A. MacLean. 1999. "Multiple geochemical and isotopic approaches for assessing groundwater NO_3^- elimination in riparian zones." *Ground Water*, 37(3), 448-457.

Nayfeh, A. H. 1981. *Introduction to Perturbation Techniques*. John Wiley & Sons, New York.

Overbeck, R.M. and T.H. Slaughter, 1958. The ground-water resources *in* The water resources of Cecil, Kent and Queen Anne's Counties: Maryland Department of Geology, Mines and Water Resources Bulletin 21, 478 p.

PeterJohn, W. T., D. L. Correll. 1984. "Nutrient dynamics in an agricultural watershed: Observations on the role of a riparian forest." *Ecology*. 65(5), 1466-1475.

Postma, D., C. Boesen, H. Kristiansen, and F. Larsen, 1991. "Nitrate reduction in an unconfined sandy aquifer: Water chemistry, reduction processes, and geochemical modeling." *Water Resour. Res.* 27(8), 2027-2045.

Reilly, T. E., L. N. Plummer, P. J. Phillips, and E. Busenberg, 1994. " The use of simulation and multiple environment tracers to quantify groundwater flow in a shallow aquifer." *Water Resour. Res.* 30(2), 421-433.

Trudell, M. R., R. W. Gillham, and J. A. Cherry, 1986. "An in-situ study of the occurrence and rate of denitrification in a shallow unconfined sand aquifer." *J. Hydrol.*, 86, 251-268.

U.S. Environmental Protection Agency, 1992. Progress Report of the Baywide Nutrient Reduction Reevaluation. U. S. Environmental Protection Agency, Chesapeake Bay Program Office, 68 pp.

Yates, P. and J. M. Sheridan, 1983. "Estimating the effectiveness of vegetated floodplains/ wetlands as nitrate-nitrite and orthophosphorus filters." *Agriculture, Ecosystems and Environment*, 9, 303-314.

Glossary

Riparian zones: are areas of vegetation (e.g., grasses, shrubs, trees, and other vegetation types) that are adjacent to bodies of water (e.g., streams).

Aquifer: is a geologic formation, or a group of formations, which (i) contains water and (ii) permits significant amounts of water to move through it under ordinary field conditions.

Unconfined aquifer: is an aquifer in which the water table forms the upper boundary. Also referred to as *phreatic aquifer* or *water-table aquifer.*

Water table: is an imaginary surface at all points of which the pressure is atmospheric (taken as zero). Also referred to as *phreatic surface.*

Hydraulic head: is energy per unit weight; it is equal to the elevation at any point in the porous medium relative to an arbitrary elevation (elevation head) plus the pressure divided by the specific weight of the fluid (pressure head). Or it is the fluid potential at any point in the porous medium divided by the gravitational acceleration. Fluids flow in the direction of decreasing heads in porous media.

Hydraulic conductivity: is the constant of proportionality between the specific discharge and the hydraulic head gradient in the Darcy's law. It can also be defined as the Darcys velocity (specific discharge) under unit hydraulic head gradient at any point in the porous medium. It depends on properties of both the porous matrix and the fluid. Some authors call it *coefficient of permeability.*

Oxic zone: is referred to here as the zone of relatively oxidized non-calcareous portion of the surficial Columbia\Aquia aquifer.

Redox zone: is referred to here as the zone of relatively reduced calcareous glauconitic sediments, which constitutes the lower boundary of the surficial aquifer. It is the zone of reduction-oxidation reaction (redox) where nitrate is reduced by denitrification.

Denitrification: refers to the microbially mediated process whereby nitrate (NO_3^-) is reduced to nitrous oxide (N_2O) or nitrogen gas (N_2) under anaerobic conditions.

Hydrostratigraphic unit: is a geologic formation, part of a formation, or a group of formations in which there are similar hydrologic characteristics that allow for a grouping into aquifers and associated confining layers.

Watershed: is a topographically defined area drained by a river/ stream or a system of connecting rivers/ streams such that all outflow is discharged through a single outlet. It can also be referred to as *drainage basin.*

Transect length: is referred to here as the horizontal distance from the upgradient drainage divide boundary to the downgradient stream boundary.